Stony Brook University

OFFICIAL COPY

The official electronic file of this thesis or dissertation is maintained by the University Libraries on behalf of The Graduate School at Stony Brook University.

© All Rights Reserved by Author.

Advances in the Structural Characterization of Duplex DNA Containing 3-Aminobenzanthrone

A Thesis Presented

By

Freda Charlotte Sansaricq

to

The Graduate School

In Partial Fulfillment of the

Requirements

for the Degree of

Master of Science

In

Chemistry

Stony Brook University

May 2009

Stony Brook University

The Graduate School

Freda Charlotte Sansaricq

We, the thesis committee for the above candidate for the

Master of Science degree, hereby recommend

acceptance of this thesis.

Dr. Carlos de los Santos - Advisor
Department of Molecular and Cellular Pharmacology

Dr. Daniel P. Raleigh - Chairperson of Defense
Department of Chemistry

Dr. Michelle Millar - Third member
Department of Chemistry

This thesis is accepted by the Graduate School

Lawrence Martin
Dean of the Graduate School

Abstract of the Thesis

Advances in the Structural Characterization of Duplex DNA Containing 3-Aminobenzanthrone

by

Freda Charlotte Sansaricq

Master of Science

in

Chemistry

Stony Brook University

2009

3-nitrobenzanthrone (3-NBA), a member of the nitrated polycyclic aromatic hydrocarbons, has been identified as an environmental pollutant and known mutagen[1]. Additionally, when introduced into mammalian cells, 3-nitrobenzanthrone forms DNA-damaging species that are potentially carcinogenic[2]. Therefore, its structural characterization is pivotal in understanding its role as a mutagen and as a substrate in the DNA repair pathway. Since structure and function are closely interrelated, structurally identifying 3-nitrobenzanthrone incorporated into duplex DNA may prove to be promising in further delineating the relationship between DNA damage and repair. Structural characterizations of 3-nitrobenzanthrone using spectroscopic and thermodynamic methods have been performed on an unmodified 11-mer duplex DNA serving as a control for comparative studies of the same duplex containing 3-aminobenzanthrone (a reduced form of 3-nitrobenzanthrone.) The characterization of the unmodified duplex proved successful; however, problems arose with the structural characterization of the damaged duplex. This thesis details the issues arising with the structural characterization of duplex DNA containing 3-aminobenzanthrone and new experiments fashioned in an attempt to address those issues.

Table of Contents

List of Symbols and Abbreviations

α	**ratio of DNA in duplex form to random coil form**
1D	**one-dimensional**
A	**adenine**
AAF	**acetylaminofluorene**
3-ABA	**3-aminobenzanthrone**
C	**cytosine**
C#	**carbon followed by numbered position**
COSY	**correlation spectrum**
COSY45	**correlation spectrum with a 45 degree reading pulse**
C_t	**total concentration**
dA	**deoxyadenosine**
dC	**deoxycytosine**
dG	**deoxyguanosine**
dG (*N*2)-AAF	**3-(deoxyguanosin-*N*2-yl)-2-acetylaminofluorene**
DMT	**dimethoxytrityl**
DNA	**deoxyribonucleic acid**
DQF-COSY	**double quantum filtered correlation spectrum**
EDTA	**ethylenediaminetetraacetic acid**
FID	**free induction decay**
G	**guanine**
ΔG°	**Gibbs free energy at given conditions**
ΔH°	**van't Hoff enthalpy**
HPLC	**high performance liquid chromatography**
K_{eq}	
mM	**millimolar (unit of concentration)**
N#	**nitrogen followed by numbered position**
3-NBA	**3-nitrobenzanthrone**
NER	**nucleotide excision repair**
nitro-PAH	**nitrated polycyclic aromatic hydrocarbon**
NMR	**nuclear magnetic resonance**
NOE	**nuclear Overhauser effect**
NOESY	**nuclear Overhauser effect spectrum**
NPE	**nitrophenylethyl**
OD_{260}	**optical density at 260 nm**
ppm	**parts per million**
R	**ideal gas constant (8.31 J/K mol)**
RNA	**ribonucleic acid**
RPA	**replication protein A**
ΔS°	**entropy at standard conditions**
T	**thymine**
T_m	**melting temperature**
TFIIH	**Transcription Factor II H**

TOCSY	**total correlation spectrum**
TSP	**trimethylsilyl-2,2,3,3-tetradeuteropropionic acid**
UV	**ultraviolet**
W-C	**Watson-Crick**
XPA	**xeroderma pigmentosum complementation group A protein**
XPB	**xeroderma pigmentosum complementation group B protein**
XPC	**xeroderma pigmentosum complementation group C protein**
XPC-HR23B	**xeroderma pigmentosum group C protein complexed to human homologue of the yeast RAD23 protein**
XPD	**xeroderma pigmentosum complementation group D protein**
XPG	**xeroderma pigmentosum complementation group G protein**

List of Figures

List of Tables

Introduction

3-NBA deleterious effects on mammalian cells can be fully appreciated with an understanding of the DNA repair mechanism. The following section details the chief pathway mammalian cells employ to repair bulky adducts in DNA; specifically, the nucleotide excision repair system.

Nucleotide Excision Repair System

There are five classes of DNA repair including nucleotide excision repair, base excision repair, direct damage reversal, mismatch repair, and double strand break repair. Nucleotide excision repair (NER) is a DNA repair mechanism used in all mammalian cells. Enzymes involved with NER, are responsible for recognizing perturbations in DNA double helix or bulky adducts that arises from damage to the DNA. NER system can be subdivided into the global genomic NER and transcription coupled NER. Global genome NER repairs damage in transcribed and untranscribed DNA strands in genes, whether or not they are active. Transcription coupled NER normally occurs while a gene is being transcribed and is initiated by recognition of RNA Polymerase II. Two different set of enzymes are utilized initially in the two types of NER.

The first step in global genome NER is recognition of the lesion in DNA helix by XPC-HR23B (the XPC protein complexed with the human homologue of *Sacchoromyces cerevisiae* Rad23, a species of budding yeast). XPC-HR23B supports the DNA conformation until the next NER factor is recruited, TFIIH (a ten-subunit complex). TFIIH contains a cdk activating kinase and a complex of proteins: XPB, XPD, p62, p34, p52, p8. XPB and XPD are the two helicases responsible for opening DNA. Following this opening, three more proteins are recruited including RPA, XPA and XPG which stabilizes the DNA in a conformation that allows for excision of the adduct along with a short segment of single-stranded DNA.

The last protein factor to be recruited is the ERCC1-XPF which performs the cut of the segment on the 5' side while XPG performs the cut on the 3' side. This leaves a hole on the single strand of the DNA that is later filled by DNA polymerase, an enzyme that catalyzes the polymerization of deoxyribonucleotides opposite a template DNA strand. Now, that we understand how the nucleotide excision pathway function, the next question to ask is: what factors are necessary for mammalian cells to initially recognize damage?

Damage Recognition in NER Pathway

In order to fully understand the NER mechanism, it is essential to describe what parameters may necessitate recognition. There are a few current hypotheses on how damage is recognized by the NER system. In 1997, Naegeli and coworkers published findings describing what was termed a "bipartite" model of NER recognition[4]. Experiments were performed on DNA duplexes with a C4'-modified backbone residue, short segments of mispaired residues, and a combination of both types of modifications.

It was found that modifying the backbone residue of a DNA duplex or incorrect base pairing alone was not sufficient for NER recognition; however, the combination of both types of disturbances proved to be the requirements needed for initiation. The model is termed bipartite because two requirements are needed for recognition by the NER, 1. Chemical modification of a nucleotide segment and 2. Incorrect Watson-Crick base pairing.

In 2002, another hypothesis came out from Geacintov and coworkers coined the "multipartite" model[5]. This expanded on the bipartite model to include other factors that may be involved in NER recognition including differences in thermodynamic properties and thermal stability as compared to normal duplex DNA. In other words, the NER system thermodynamically scans DNA in search of instability. This instability is thought to be attributed to structural differences in irregular DNA as compared to normal DNA and can be measured through such structural parameters as degree of propeller twist, rise or buckle, hydrogen bond distances, bending, stacking, changes in helical backbone torsional angles, etc. Ultimately, this means that structural differences in the DNA duplex lead to the initiation of the NER mechanism.

3-(deoxyguanosin-*N*2-yl)-2-acetylaminofluorene (dG (*N*2)-AAF) demonstrates an interesting case study in its role as a substrate for the NER pathway. This lesion present in duplex DNA has special properties. From a structural point of view it has a defined configuration that does not distort the duplex and maintains Watson-Crick (W-C) base pair alignment[6]. The lesion, located in the minor groove, follows the double helix curvature well and is protected from solvent exposure. In addition, it stabilizes the double helix thermodynamically (Note: helix-stabilizing lesions are not common). It has been documented from previous experiments that the N2 adduct remains in the cell for a long time[7, 8]**.** This can be explained partly due to the fact that dG (*N*2)-AAF adduct may not be a substrate for NER. According to the multipartite model, which affirms that NER efficiency goes down when the helix is stabilized and base-paring is normal, the dG (*N*2)-AAF adduct is expected to not be recognized by the NER system. For a lesion to be an effective substrate of NER, it must exhibit perturbations of W-C alignment or distortions of other helical parameters. In light of this, the study of the N2 adduct of 3-nitrobenzanthrone should be especially informative since the two lesions demonstrates similar geometries. Investigation of 3-nitrobenzanthrone may prove to deliver similar results as obtained from the study of dG (*N*2)-AAF. The results of this investigation may lead to an answer of the overriding question if whether or not 3-nitrobenzanthrone is a substrate for NER.

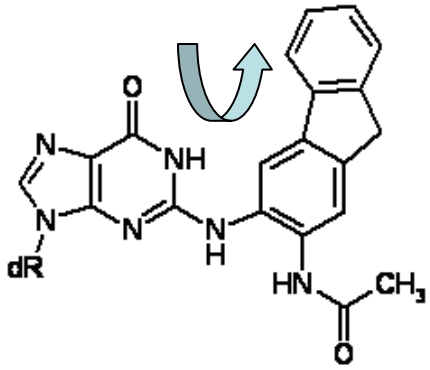

Figure I-1: Chemical structure of dG(N2)-AAF adduct. The arrow identifies the analogous geometry that the adduct shares with the dG(N2)-3-ABA adduct.

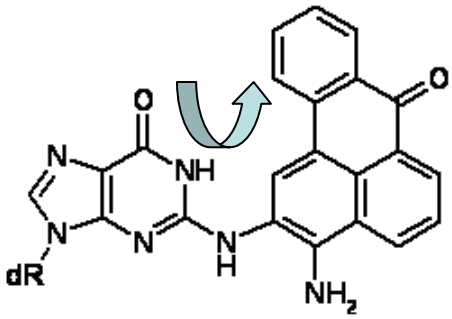

Figure I-2: Chemical structure of dG(N2)-3-ABA adduct. The arrow identifies the analogous geometry that the adduct shares with the dG(N2)-AAF adduct.

Structure of 3-nitrobenzanthrone

3-Nitrobenzanthrone [3-nitro-7H-benz[de]anthrace-7-one], chemical formula $C_{19}H_9NO_3$ (3-NBA) is part of a family of molecules identified as nitrated polycyclic aromatic hydrocarbons (nitro-PAHs) that are found commonly in the environment derived from diesel exhaust, river sediments or food[1]. Nitro-PAHs have the general structure of multiple aromatic benzene rings combined with a nitrated constituent. All 3-NBA-derived DNA adducts are formed by nitroreduction and are bound to a deoxyadenosine (dA) or deoxyguanosine (dG), without carrying an N-acetyl group. Adducts formed from 3-NBA are usually linked at the C8 and N^2 position of dG or the C8 and N^6 position of dA.

dG-C8

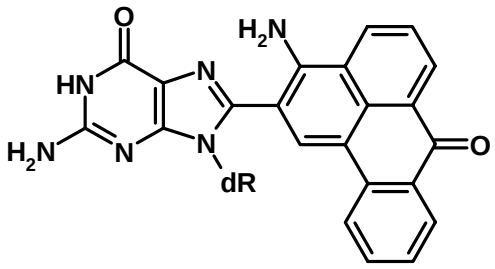

dG-N^2

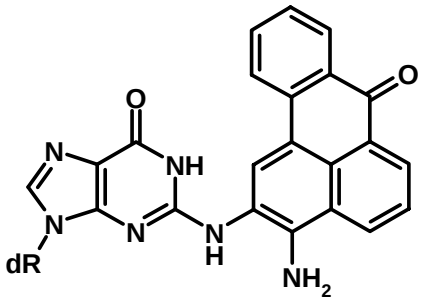

dA-N6

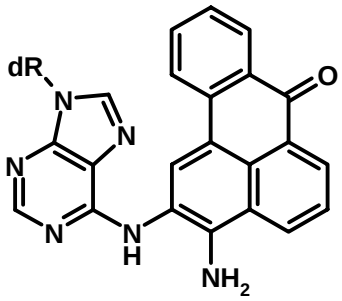

dG-C8

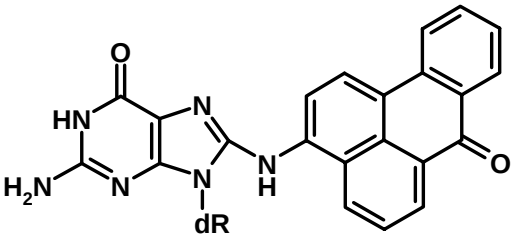

Figure I-3: Chemical structures of DNA adducts formed from 3-nitrobenzanthrone.

Significance of 3-nitrobenzanthrone

As determined in multiple studies using the Ames Salmonella assay[9], many members of the Nitro-PAHs family are highly mutagenic and some are suspected carcinogens. They are a focus of concern since they are found throughout the environment and pose possible human health risks. Nitro-PAHs are the by-products of incomplete combustion as formed from vehicle exhaust, smoking, heating, certain food processing, etc.[10, 11, 12] Additionally, they are suspected to be formed from the combustion of aromatic hydrocarbons and nitrogen dioxides under atmospheric conditions as shown through some experimental studies.[1, 13] Nitro-PAHs must undergo some sort of metabolism to form an electrophilic species that chemically reacts with DNA to form various adducts. 3-NBA's concentration in the atmosphere is comparable to another Nitro-PAH, 1, 8-dinitropyrene, a common environmental pollutant and known mutagen with comparable potency. Its chief metabolite, 3-aminobenzanthrone (3-ABA), is detectable in the urine of salt mine workers that are in contact with diesel exhaust.[14, 15]. Other metabolites identified include 3-acetylaminobenzanthrone (3-Ac-ABA) and N-acetyl-N-hydroxy-3-aminobenzanthrone (N-Ac-N-OH-ABA)[25] 3-NBA was first reported to be found in significant concentrations within organic extracts of diesel exhaust and airborne particles[1], where its formation was speculated to be the result of combustion processes of fossil fuels and reactions of hydrocarbons with nitrogen oxides in the air. Concomitant to its discovery, it was found to be highly mutagenic by an Ames Salmonella assay (208,000 revertants / nmol in *Salmonella typhimurium* TA98 and 6,290,000 revertants / nmol in YG1024) and it was found to stimulate micronuclei (chromosome fragments that are not incorporated into the nucleus at cell division) production in mouse peripheral blood reticulocytes implicating that it may be toxic to mammalian cells. Through previous studies, it is documented that human exposure to air pollutants and diesel exhaust is linked with an increased risk for lung cancer[9, 14].

Chemistry of 3-nitrobenzanthrone (in vivo studies)

Through ^{32}P-postlabelling assay, Arlt et. al[15] were able to propose a potential pathway of metabolic activation. 3-NBA is proposed to undergo nitroreduction to form N-hydroxy-3-aminobenzanthrone (N-OH-ABA); the enzymes catalyzing this reaction are cytosolic reductases and a microsomal oxidoreductase; however as determined by an independent study[16], nitroreduction of 3-NBA is accomplished predominantly by cytosolic reductases. N-OH-ABA can also be formed through N-oxidation of 3-NBA's metabolite 3-ABA, catalyzed by cytochrome P450 enzymes (CYP). N-OH-ABA can form the reactive esters through activation by phase II enzymes, n-acetyltransferases or sulfotransferases (NAT1, NAT2, SULT1A1, and SULT1A2). The reactive esters form nitrenium ions that react with DNA to give non-acetylated 3-NBA-derived DNA adducts.
Another pathway N-OH-ABA can take is to form N-acetyl-N-hydroxy-3-aminobenzanthrone which undergoes O-acetylation or O-sulfonation to form a reactive ester that leads to the N-acetyl nitrenium ion that eventually reacts with DNA to yield acetylated 3-NBA derived adducts.

Studies involving 3-nitrobenzanthrone demonstrated its metabolic activation in vivo by human acetyltransferases, sulfotransferases and cytochrome P450 human enzymes.[17,18] In these studies, human N,O-acetyltransferases' and sulfotransferases' biological roles in 3-NBA's activation were examined in Chinese hamster lung fibroblast V79MZ-h1A2 cells expressing human CYP1A2 (cytochrome P450 enzymes). V79 cell lines are commonly used in mutagenicity testing and mechanistic studies of mutagens; partly because of its short generation time of 12 hours. In this study it was specifically utilized because the V79 derived Chinese hamster fibroblasts do not have endogenous cytochrome P450 dependent or sulfotransferase/ acetyltransferase enzyme activity. In different cells they expressed a human N, O-acetyltransferase or human sulfotransferase in order to investigate its role in activation. Cell genotoxicity substantially increased with the addition of 3-NBA in either cells containing the sulfotransferase or acetyltransferase as compared to the addition of 3-NBA to just the parent cell expressing the human cytochrome enzyme alone. Results implied that both types of enzymes in conjunction with human cytochrome P450 enzymes are necessary for the metabolic activation of 3-NBA as was seen in the increased toxicity of cells expressing the N, O-acetyltransferase or the sulfotransferase upon addition of 3-NBA as compared to the parent cells lacking these enzymes. To reiterate, the current hypothesis is that metabolic activation of 3-NBA consists of either an initial nitroreduction step followed by O-acetylation catalyzed by human acetyltransferases or an initial nitroreduction step followed by O-sulfonation catalyzed by human sulfotransferases.

In vivo studies involving ^{32}P-postlabeling analyses of DNA of several organs from rats that were administered 3-NBA orally, demonstrated the existence of the same types of adducts as are found from in vitro experiments.[19] In the same study 3-NBA and its metabolites are speculated to circulate through the bloodstream, as adducts appeared in organs such as the kidney, liver and lung, outside of the digestive tract. Additionally, it was confirmed that metabolic activation of 3-NBA involves nitroreduction rather than ring oxidation.

In studies involving rat lung alveolar type II cells, rat bronchial epithelial cells, rat mesenchymal cells, and human fetal bronchial cells incubated with 3-nitrobenzanthrone in periods of time that spanned less than a day, 3-Aminobenzanthrone was identified as the major metabolite of 3-nitrobenzanthrone.[11] The identification of this metabolite was further confirmed through the discovery of 3-Aminobenzanthrone in the urine of salt mine workers[20].

Nucleic Magnetic Resonance Experiments

Two-dimensional NMR experiments are composed of four time periods: preparation, evolution, mixing, and detection. During the preparation period coherence is created through the generation of one or few radiofrequency pulses. Evolution time period consists of an evolution of the coherence to assume a specific state. Following this, the mixing period transfers the coherence between spins through radiofrequency pulses and delays. Finally, the detection period results in a free induction decay (FID) that is

recorded. All two-dimensional NMR experiments including NOESY, COSY, TOCSY, etc. are variations of the evolution and mixing time periods.

The primary NMR experiment utilized for structural determination is a two dimensional nuclear Overhauser enhancement and exchange spectroscopy (NOESY) experiment, whose mixing period has two 90º pulses that are separated by a mixing time τ_m. NOESY, H_2O-NOESY, COSY and TOCSY experiments were used for assignment of non-exchangeable and exchangeable protons.

Thermodynamics and Thermal Stability of Nucleic acids

Characterizing the thermodynamics of the DNA duplex involves generation of the Van't Hoff thermodynamic parameters. The below discussion will detail the derivations[23, 24]: Standard state free energy can be related to the equilibrium constant as

$$\Delta G^o = - RT \ln K_{eq} \quad \textbf{(1)}$$

R = 8.31 J/K * mol (gas constant)
T = Temperature (Kelvin)

Standard state free energy can also be related to enthalpy and entropy changes as

$$\Delta G^o = \Delta H^o - T\Delta S^o \quad \textbf{(2)}$$

Changes in the temperature, at constant pressure, can be shown in the aforementioned equations respectively as

$$\frac{\delta}{\delta T}\left(\frac{\Delta G^\circ}{T}\right)_P = -R\left(\frac{\delta \ln Keq}{\delta T}\right)_P \quad \textbf{(3)}$$

$$\frac{\delta}{\delta T}\left(\frac{\Delta G^\circ}{T}\right)_P = -\frac{\Delta H^\circ}{T^2} \quad \textbf{(4)}$$

By combining these two equations we get the van't Hoff equation:

$$\Delta H^\circ_{vH} = RT^2\left(\frac{\delta \ln K_{eq}}{\delta T}\right)_P \quad \textbf{(5)}$$

T_m is the temperature at which one half of a complex is disassembled or in this case, there is an equal ratio between helical (double stranded DNA) and random coil (single-stranded) DNA. If one defines α as the fraction of duplex DNA, then T_m can be defined as the point when α = 1/2.

$$K_{eq} = \frac{\alpha}{(1-\alpha)} \quad \textbf{(6)}$$

Or, because we are interested in a bimolecular process:

$$K_{eq} = \frac{\alpha\left(\frac{C_T}{n}\right)}{\left(\left(1-\alpha\right)\left(\frac{C_T}{n}\right)\right)^n} = \frac{\alpha}{\left(1-\alpha\right)^n\left(\frac{C_T}{n}\right)} \quad \textbf{(7)}$$

With α = fraction of unfolded duplex DNA and n = molecularity.

Substituting this equation into the van't Hoff equation yields the following equation:

$$\Delta H^{\circ}_{vH} = 6RT_m^2\left(\frac{\delta\alpha}{\delta T}\right)_{T=T_m} \quad \textbf{(8)}$$

Therefore, the van't Hoff enthalpy can be determined from the shape of the melting curve at the melting temperature T_m from a plot of α versus T.
Equation **(7)** can be further reduced since the molecularity of the reaction is two (molecularity of duplex DNA separated into its component strands is two) and we are interested in T_m at α = 1/2:

$$K_{T_m} = \frac{4}{C_T} \quad \textbf{(9)}$$

Substituting this into the following equations (1) and (2):
$\Delta G^\circ = -RT\ln K = \Delta H^\circ - T\Delta S^\circ$
yields

$$-RT_m \ln\left(\frac{4}{C_T}\right) = \Delta H^\circ - T_m\Delta S^\circ \quad \textbf{(10)}$$

Which can be re-arranged into a standard line equation y = mx + b as

$$\frac{1}{T_m} = \frac{R}{\Delta H^\circ}\ln\left(\frac{C_T}{4}\right) + \frac{\Delta S^\circ}{\Delta H^\circ} \quad \textbf{(11)}$$

Plotting $\frac{1}{T_m}$ versus $\ln\left(\frac{C_T}{4}\right)$ gives a slope of $\frac{R}{\Delta H^\circ}$ and an intercept of $\frac{\Delta S^\circ}{\Delta H^\circ}$.
R is the ideal gas constant and is equal to 1.987 cal/mol K.

Materials and Methods

Synthesis and purification of the unmodified 11-mer duplex

C_1 G_2 T_3 A_4 C_5 G_6 C_7 A_8 T_9 G_{10} C_{11}

G_{12} C_{13} A_{14} T_{15} G_{16} C_{17} G_{18} T_{19} A_{20} C_{21} G_{22}

Figure II-1: Sequence of unmodified 11mer duplex DNA

The unmodified 11-mer duplex was synthesized at the SUNY Stony Brook DNA synthesis facility. To purify strands, samples were injected into a Gilson HPLC system equipped with a manometric module and gradient pump (306). HPLC, a form of liquid chromatography, was used to separate the two DNA strands dissolved in the solution. In this case**,** the two mobile phases utilized were 50% acetonitrile/ 50% deionized water and 50% triethylammonium/ 50% deionized water. The HPLC system successfully resolved the two single stranded DNA molecules.

Samples were frozen at -70º C and then placed into lyophilizer for 24 hours to complete drying. A 1:1 stoichiometric ratio of the two strands was calculated for correct base-pairing. Beer-Lambert's law was used to determine volume amount of each strand necessary to attain a 1:1 stoichiometric ratio of duplex DNA.

Beer-Lambert's law:
$A = \varepsilon bc$ where **ε** is the extinction coefficient, **b** is the path length, and **c** is the concentration.
Generunner v3.99 (Hastings Software Inc.) was used to calculate epsilon coefficients:
$nMol / A_{260} = 1/\varepsilon$

Top strand: CGTACGCATGC
$1/\varepsilon = 9.9$ mMol/ A_{260}
$\varepsilon = 1.01 * 10^2$ A_{260}/mol

Bottom strand: GCATGCGTACG
$1/\varepsilon = 9.5$ mMol/ A_{260}
$\varepsilon = 1.05 * 10^2$ A_{260}/mol

The UV spectrum was obtained for both strands using a Shimadzu UV160U Spectrophotometer. 10 microliters of the first strand in EDTA solvent produced an OD of 0.804 and 10 microliters of the second strand in water produced an OD of 0.643.

The UV spectrum for first strand after removal of EDTA solvent was obtained as well with 10 microliters producing an OD of 0.791. The two strands were then separately dissolved in 2 mL of deionized water. Four determinations of UV reading were taken of the strands with a concentration of 5, 10, 15, 25 microliters in order to determine the absorption units per volume of solution. The absorption unit per volume of each strand was derived from the slope of absorbance versus concentration plot.

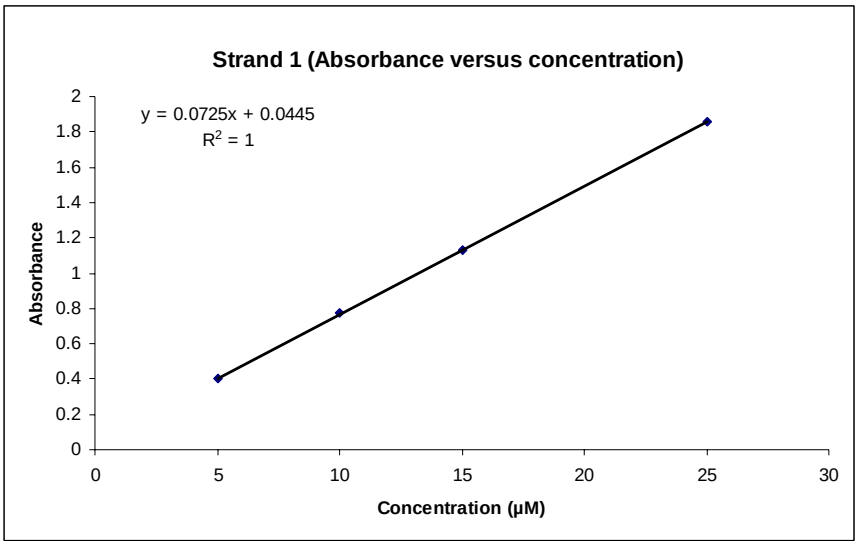

Figure II-2: Graph of the first oligonucleotide strand of the unmodified 11-mer duplex at varying concentrations and absorbance

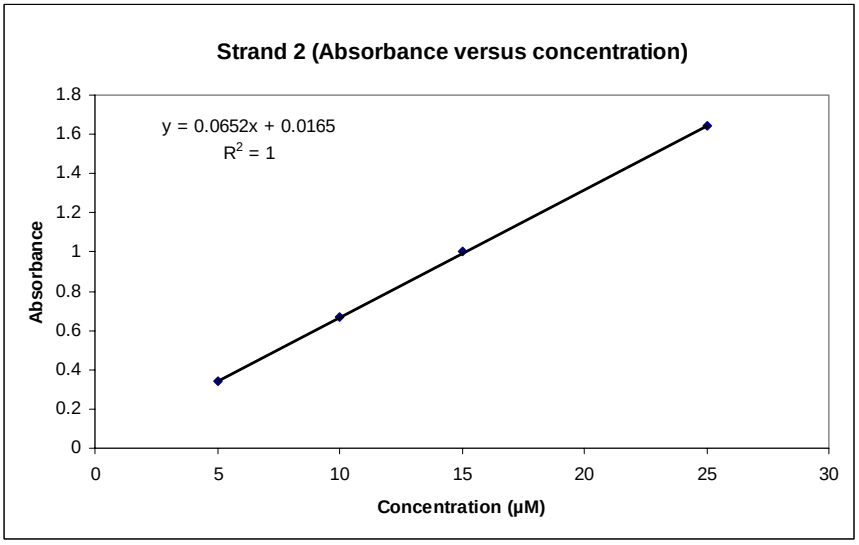

Figure II-3: Graph of the second oligonucleotide strand of the unmodified 11-mer duplex at varying concentrations and absorbance

$$\frac{\text{Moles 1}}{\text{Volume 1}} = \frac{\text{Abs (1)}}{\varepsilon_1}$$

$$\frac{\text{Moles 2}}{\text{Volume 2}} = \frac{\text{Abs (2)}}{\varepsilon_2}$$

Moles 1 = Moles 2 →

$$\frac{\text{Volume 1} * \text{Abs (1)}}{\varepsilon_1} = \frac{\text{Volume 2} * \text{Abs (2)}}{\varepsilon_2}$$

$$\frac{\text{Volume 1} * \text{Abs (1)/microliters}}{\text{Abs (1)/moles 1}} = \frac{\text{Volume 2} * \text{Abs (2)/microliters}}{\text{Abs (2)/moles 2}}$$

$$\frac{\text{Volume 1} * \text{moles 1}}{\text{microliters}} = \frac{\text{Volume 2} * \text{moles 2}}{\text{microliters}}$$

Calculating DNA Concentration

OD = Optical Density

Strand 1: $\frac{0.072\ OD_{260}\ /\ \mu L}{0.101\ OD_{260}\ /nmol} = 0.72 \times 10^{-3}$ mol/L

Strand 2: $\frac{0.065\ OD_{260}\ /\ \mu L}{0.105\ OD_{260}\ /nmol} = 0.62 \times 10^{-3}$ mol/L

1.5 mL Strand 2 was added to 1.3 mL of Strand 1

Strands were combined with the appropriate aforementioned 1:1 stoichiometry to create a duplex DNA sample. After mixing, the duplex DNA sample was heated from 80ºC to 95°C. Heat was then removed from the system to allow slow cooling and proper annealing. Afterwards sample was lyophilized and 0.6 mL of D_2O was added in preparation for NMR spectroscopic Studies.

Synthesis and Purification of the unmodified 14-mer duplex

G_1 T_2 A_3 T_4 G_5 C_6 C_7 G_8 G_9 C_{10} A_{11} T_{12} A_{13} C_{14}

Figure II-4: Sequence of unmodified 14mer duplex DNA

The unmodified 14-mer duplex was synthesized at the SUNY Stony Brook DNA synthesis facility using solid state synthesis. Sequences containing an O-5'-dimethoxytrityl group were isolated by treatment with ammonium hydroxide (14.8 M) and purified by reverse phase HPLC. the mobile phase consisted of solvent 0.1 M Triethylammonium acetic acid buffer, pH 6.8, and acetonitrile. Using a linear gradient of 0 to 40% in acetonitrile in 40 minutes, the desired sequence was eluted. The O-5'-dimethoxytrityl group was cleaved by treatment with 0.5mL fractions of 80% acetic acid for 30 min and the solution extracted with ether four times before purification by HPLC. The solution was placed into a freezer at -80º C for three hours and lyophilized. Oligodeoxynucleotide sequences were desalted by passing them through a Sephadex G-25 column and converted to the sodium salt using a Dowex 50W cation exchange column.

There was apprehension that the oligonucleotide would form hairpins since the sequence is self-complementary; however, hairpins did not form for a couple of reasons. One is the presence of counter ions supplied by the NaCl in the buffer which partially neutralized the phosphate charges on the DNA, favoring the formation of duplex DNA over formation of hairpin. Also because of the law of mass action the equilibrium was shifted towards formation of duplex DNA. Since the sample had a concentrated amount of oligonucleotides that are in close proximity to each other, one strand of the oligonucleotide was more likely to partner with another strand of the oligonucleotide versus folding unto itself.

Synthesis of 3-aminobenzanthrone-N^2-dG adduct:

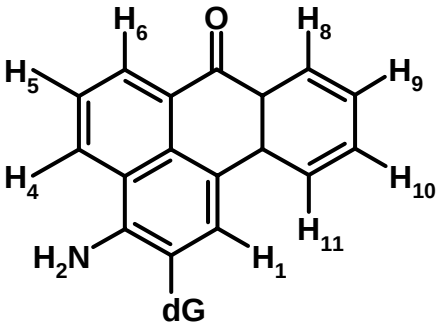

Figure II-III: Chemical structure of 3-aminobenzanthrone with numbering scheme

The synthesis of the 3-aminobenzanthrone-N^2-dG adduct and its incorporation into the 14-mer oligonucleotide was performed by Dr. Mark Lukin. The synthetic scheme is reported elsewhere[21]. A brief outline is presented here. The starting materials were a bromo derivative (prepared from 3-nitrobenznathrone that underwent reduction, bromination, deamination and nitration to produce the final derivative) and a protected nucleoside. The O^6 group of the nucleoside was protected with nitrophenylethyl (NPE) and the oxygens on the 3' and 5' carbons of the deoxyribose were protected with a silyl group. The two initial reactants were coupled in the presence of a palladium catalyst, Pd_2dba_3, xantphos and Cs_2CO_3 (cesium carbonate).

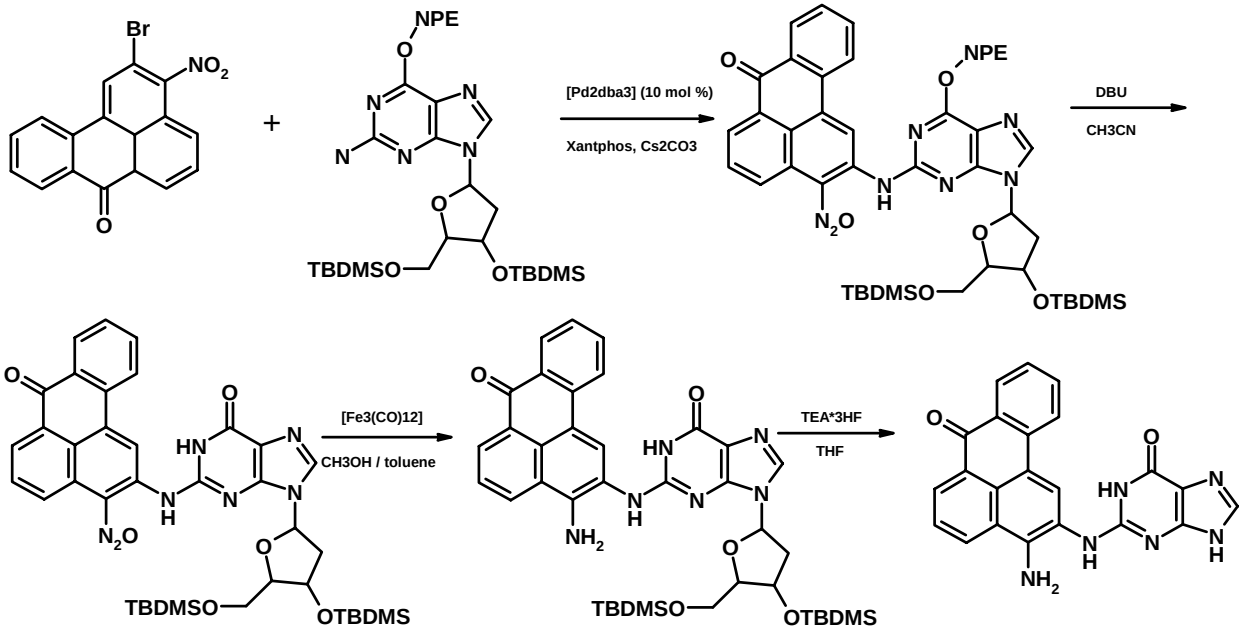

Figure II-IV: Synthetic Scheme of dG(N2)-3-ABA adduct

The NPE was selectively deprotected from the O^6 group of the nucleoside with 1,8-diazabicyclo[5.4.0]undec-7-ene (DBU) with acetonitrile (CH_3CN). The nitric oxide group on the benzanthrone moiety was selectively reduced with the use of $[Fe_3(CO)_{12}]$ (eisencarbonyl) in methanol/toluene. Finally, the silyl protecting groups were removed from the deoxyribose with TEA*3HF (triethylamine trihydrofluoride) in tetrahydrofuran. Finally, the 3-ABA adduct was incorporated into the 6^{th} position of the 11-mer duplex and the 5^{th} position of the 14mer duplex using standard phosphoramidite chemistry.

$$C_1\ G_2\ T_3\ A_4\ C_5\ G_6^*\ C_7\ A_8\ T_9\ G_{10}\ C_{11}$$

$$G_{12}\ C_{13}\ A_{14}\ T_{15}\ G_{16}\ C_{17}\ G_{18}\ T_{19}\ A_{20}\ C_{21}\ G_{22}$$

Figure II-7: Sequence of 11mer duplex DNA containing 3-ABA. * indicates base placement of 3-ABA.

$$G_1\ T_2\ A_3\ T_4\ G_5^*\ C_6\ C_7\ G_8\ G_9\ C_{10}\ A_{11}\ T_{12}\ A_{13}\ C_{14}$$

Figure II-8: Sequence of 14mer duplex DNA containing 3-ABA. * indicates base placement of 3-ABA.

NMR experiments

NMR experiments on all duplexes were performed on a Varian (INOVA) spectrometer at 500 MHZ. ^1H chemical shifts were referenced to 3-(trimethylsilyl)-2,2,3,3,-d_4 (TSP) at 0 p.p.m. NOESY, DQF-COSY and TOCSY experiments were taken in 100% D_2O buffer at pH = 6.8 and 25º C. Mixing time for all NOESY experiments was 300 ms with the exception of the 11-mer duplex containing 3-ABA whose mixing time was 350 ms. H_2O-NOESY experiments on the unmodified 11-mer duplex were performed in 90% H_2O and 10% D_2O buffer at pH = 6.8 and 25º C. Collected NMR data were processed on FELIX98 software (Accelrys, San Diego, CA) on Silicon Graphics Work station.

NMR Thermal Denaturation

NMR experiments were performed on the unmodified 11-mer duplex in 90% H_2O buffer at 5, 10, 15, 20, 25, 30, 35, 40, 45, 50º C respectively. One-dimensional temperature dependent curves were generated to investigate thermal dependence of imino protons.

DNA Melting Experiments: Stability

DNA melting experiments were performed on the unmodified 11-mer duplex and the 11-mer duplex containing 3-ABA. Samples were dissolved in buffer solution: 25 mM NaH_2PO_4, 0.5 mM EDTA, 100 mM NaCl at pH = 6.80 and subjected to three consecutive melting experiments in a Cary 100 Bio UV-Visible Spectrophotometer: starting at 80º C, ending at 10º and repeated in the reverse direction two more times until finally ending at 10º C.

pH Dependence Melting Experiments

DNA melting experiments on the unmodified 11-mer duplex were performed at eight different pHs = 4.48, 5.13, 5.69, 6.06, 6.66, 7.11, 7.49, 8.06 and at the same concentration, 30 microliters (1 OD) were performed. Samples were dissolved in 1 milliliter of buffer solution: 25 mM NaH_2PO_4, 0.5 mM EDTA, 100 mM NaCl and subjected to three consecutive melting experiments in a Cary 100 Bio UV-Visible Spectrophotometer: starting at 80º C, ending at 10º and repeated in the reverse direction two more times until finally ending at 10º C.

Resonance Assignment Strategy: Two-Dimensional NMR Spectroscopy[22]

The Overhauser effect, first characterized by Albert Overhauser in the 1950s, is the observation that spin polarization transfers from one spin population to another occurs through cross-relaxation. The nuclear Overhauser effect (NOE) characterizes a specific case in which nuclear spins are transferred. A NOESY experiment is technique used to measure NOE and identify pairs of protons that undergo cross-relaxation. Protons that are less than 5 Å apart will show an NOE readily identified in a 2D spectrum by a peak. One can establish the conformation of DNA by measuring the distances between protons. The reliability of the determined structure depends upon how may NOE cross-peaks have been assigned correctly. The diagonal elements on a 2D spectrum represent longitudinal relaxation rates and the elements off the diagonal are cross-relaxation rates.
The non-exchangeable protons of the ^{1}H-NMR spectra were assigned based on NOESY and COSY, exercising standard methods.[1] Two-dimensional NOE experiments can be used to assign DNA duplex samples up until a certain base-pair length. Peaks on the diagonal represent the 1D spectrum of the sample and peaks off the diagonal are NOE interactions between protons less than 5Å in distance. Assignment starts in the "fingerprint region" which is the region containing the base protons of the pyrimidines (H-6) and purines (H-8), approximately 7.1 – 8.4 ppm and the H-1' sugar protons, approximately 5.3 – 6.3 ppm. NOE peaks can be seen between base protons and their own H-1' sugar protons and the 5'-flanking H-1' sugar protons. 5'-terminal residues will only display one NOE peak between its base protons and its own H-1' sugar proton. In the fingerprint region other interactions that can be seen such as that between the Adenine H2 protons and its own H-1' sugar protons as well as its 3'-flanking H-1' sugar protons

and its Watson-Crick's partner's H-1' sugar proton as well as its 3'-flanking H-1' sugar proton. Interactions can also be seen between cytosine's 5H proton with the base protons of the 5'-flanking residue. From knowing the strand sequence, it is possible to perform an NOE "walk" to identify cross peaks in the two-dimensional spectrum. H-3' protons may resonate close to the solvent and not be distinguishable in the spectrum. Exchangeable proton assignment starts with the region containing the imino and amino protons. Previously assigned adenine H2 protons facilitates in the assignment of thymine imino protons. G (N-H1) protons are assigned with the hydrogen-bonded and non-hydrogen-bonded cytosine pairs. Protons of non-hydrogen bonded GC pairs are shifted downfield as compared to their hydrogen-bonded counterparts. Other assignments are made with similar comparisons between the H_2O-NOESY spectrum and the deuterated NOESY spectrum.

Results

Unmodified 11-mer duplex

NMR characterization of the unmodified 11-mer duplex was effectively performed and results of the "NOE walk" of the base-H1' protons are presented in figures III-1 and III-2. Imino and amino protons were identified using data from an H_2O-NOESY spectrum whose contour plot is detailed in figure III-3. Chemical shift values for exchangeable and non-exchangeable protons are presented in table I.

The thermal and thermodynamic studies proved to display normal characteristics of an unmodified duplex DNA. Included in these studies was the generation of NMR-based temperature dependence curves allowing one to examine the relative thermal stability of the DNA duplex as shown in figures III-4 to 13. Following the imino protons proved that the unmodified DNA exhibited normal melting behavior in which the strands separate from the terminal base pairs inwards as demonstrated in the figure from a decreasing signal of the terminal imino protons as temperature is increased.

Thermodynamic parameters of the oligonucleotide duplex were extracted from the melting experiments of the oligonucleotide strands performed at varying concentrations as displayed in figure III-14. From a plot of T_m^{-1} versus ln (Ct/4), $\Delta H°$ was determined to be -95.5 kcal/mol, $\Delta S°$ = -0.267 kcal/mol*K, $\Delta G^{\circ}_{25°C}$ = -15.9 kcal/mol, and $\Delta G^{\circ}_{37°C}$ = -12.7 kcal/mol (table 2.) These values are comparable to those obtained from similar experiments found in published data[25].

pH dependence experiments were performed to ascertain the relative stability of the duplex dna under varying pH concentrations. The unmodified duplex DNA seems to experience an increase in stability with increasing pH as can be correlated with increasing Tm. From pH =6 – 8, the Tm does not change significantly and is measured to be around 56ºC (figure III-15.)

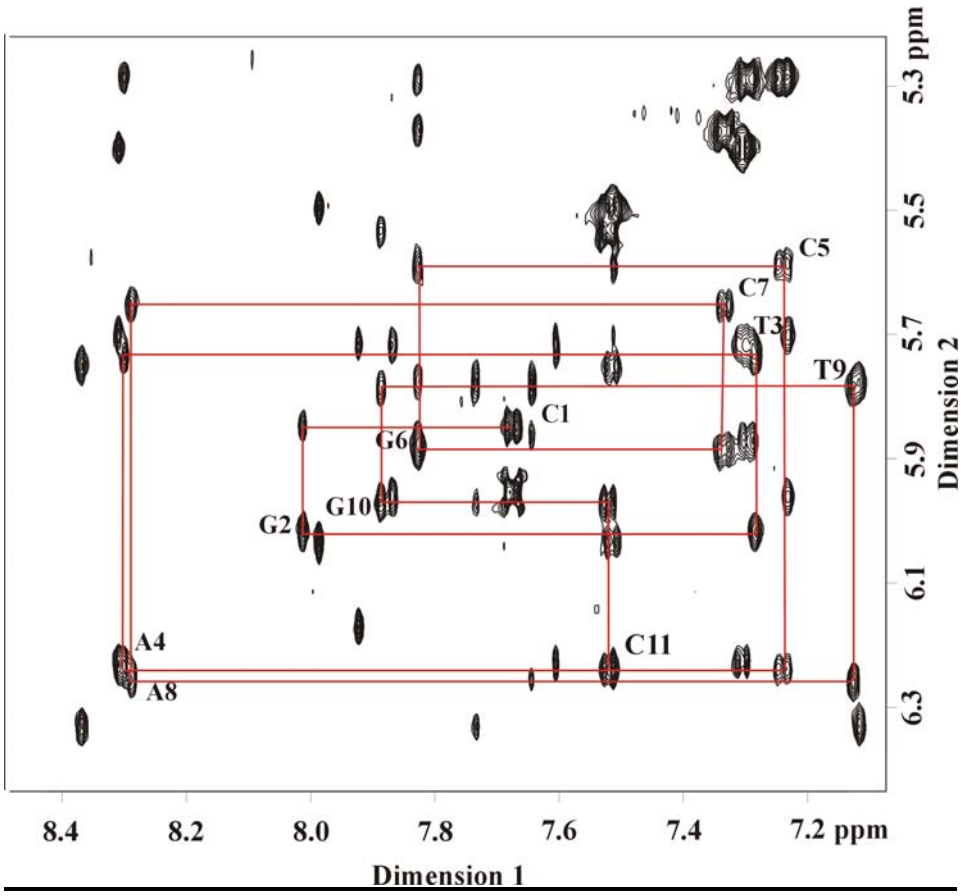

Figure III-1: Contour plot of ^{1}H NOESY spectrum (Dimension 1: Base protons (H8-purines and H6-pyrimidines); Dimension 2: H1' deoxyribose sugar protons) of the unmodified 11-mer duplex. Demonstration of the "NOE walk" for the first oligonucleotide strand

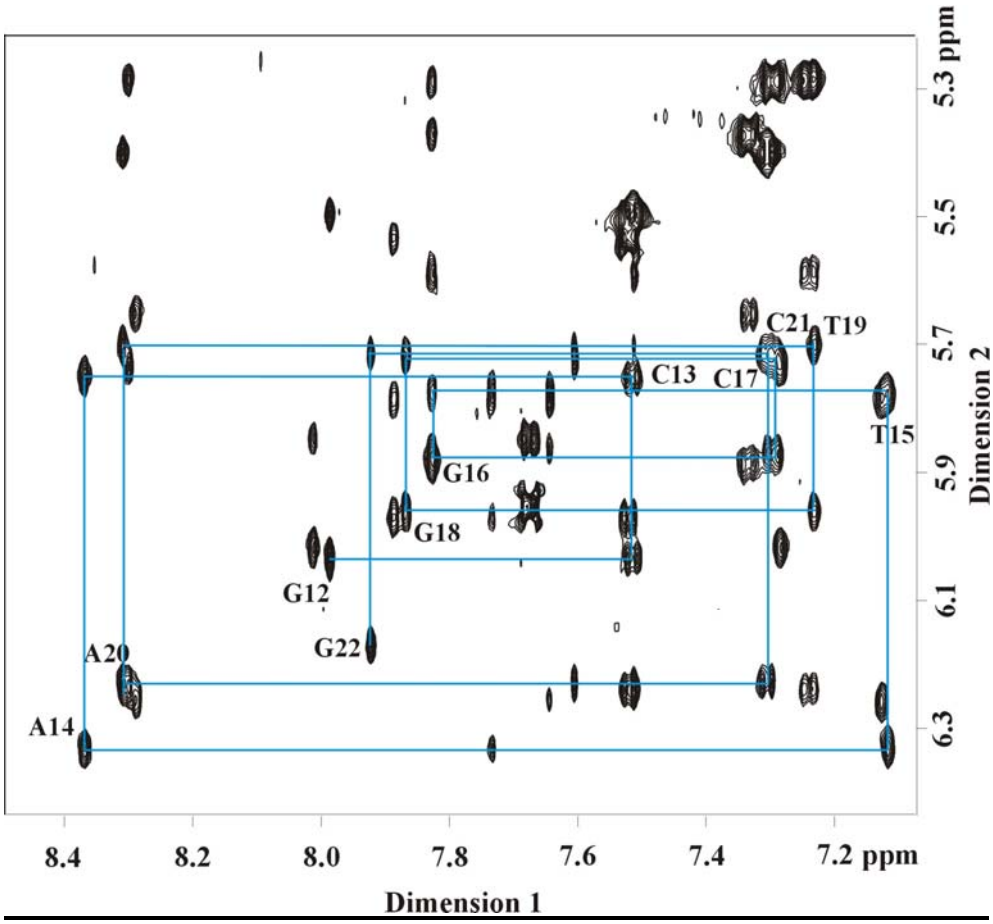

Figure III-2: Contour plot of ^{1}H NOESY spectrum of the unmodified 11-mer duplex. (Dimension 1: Base protons; Dimension 2: H1' deoxyribose sugar protons). Demonstration of the "NOE walk" for the second oligonucleotide strand.

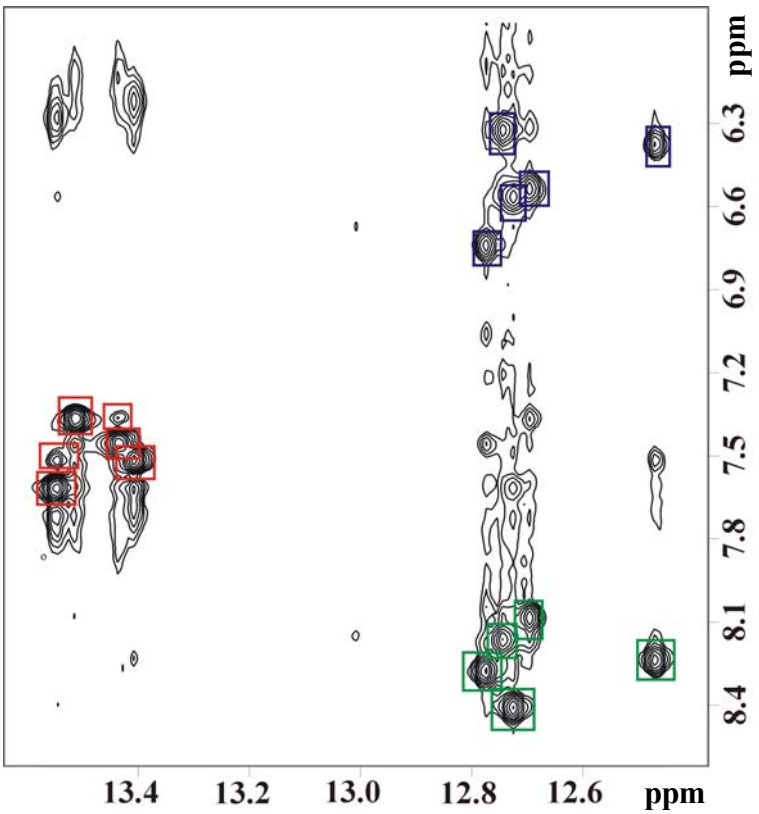

Figure III-3: Imino-Amino region of H_2O- NOESY spectrum of the unmodified 11-mer duplex. The red boxes encircle cross peaks between adenine H2 protons and thymine imino protons in the sample, the green boxes encircle cross peaks between cytosine amino protons hydrogen-bonded to guanine imino protons and the purple boxes are interactions between cytosine amino protons not participating in hydrogen bonds.

Base	H1'	H2'	H2''	H3'	H4'	H6 H8	CH3 H5 H2	CN4H GH1 TH3
C1	5.85	2.05	2.47	N/A	N/A	7.67	N/A	----
G2	6.02	2.72	2.83	5.01	4.40	8.01	----	12.8
T3	5.73	2.13	2.42	4.92	N/A	7.28	1.55	13.4
A4	6.24	2.75	2.48	5.06	4.45	8.30	7.51	----
C5	5.59	N/A	N/A	4.90	N/A	7.23	5.28	8.09
G6	5.88	N/A	N/A	4.99	4.38	7.83	----	12.7
C7	5.65	2.09	2.44	4.86	N/A	7.34	5.37	8.24
A8	6.25	2.69	2.94	5.03	4.43	8.29	7.64	----
T9	5.78	1.99	N/A	4.89	N/A	7.13	1.47	13.6
G10	5.97	2.64	2.73	5.00	4.39	7.89	----	12.7
C11	6.24	N/A	N/A	4.53	N/A	7.51	5.53	----
G12	6.03	2.65	2.83	4.89	N/A	7.99	----	----
C13	5.75	2.21	2.53	4.92	N/A	7.51	5.50	8.41
A14	6.33	2.75	3.00	5.07	4.48	8.37	7.73	----
T15	5.78	N/A	N/A	4.90	N/A	7.12	1.49	13.4
G16	5.87	N/A	N/A	4.99	4.38	7.83	----	12.5
C17	5.72	N/A	2.42	4.85	N/A	7.29	5.29	8.16
G18	5.96	N/A	N/A	4.97	4.37	7.87	----	12.7
T19	5.70	2.06	N/A	4.90	4.44	7.23	1.52	13.5
A20	6.23	2.88	2.72	5.05	N/A	8.31	7.61	----
C21	5.72	1.89	2.32	4.82	N/A	7.31	5.40	8.28
G22	6.17	2.40	2.61	4.68	N/A	7.92	----	----

Table I: Chemical shift values for unmodified 11-mer duplex measured at 25ºC. Chemical shifts are referenced to TSP. N/A: not assigned.

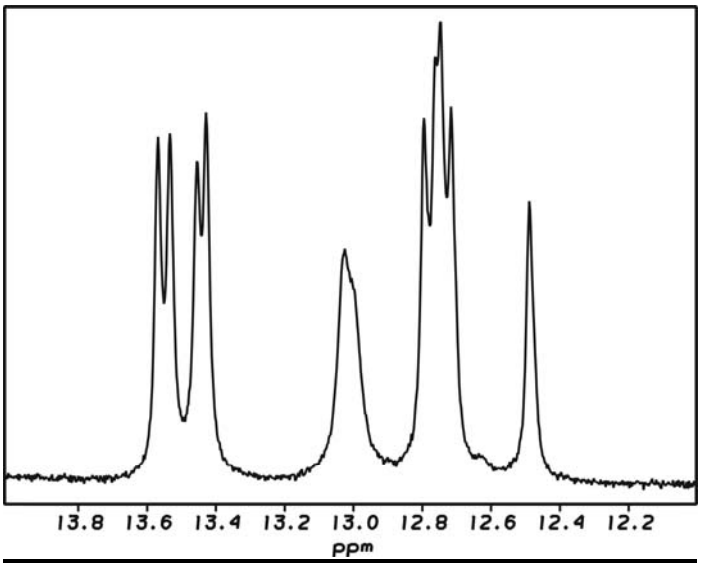

Figure III-4: One-dimensional NMR spectrum of temperature dependence experiment in 10% D_2O/ 90% H_2O, 25 mM NaH_2PO_4, 0.5 mM EDTA, 50mM NaCl buffer, pH 6.78, at 5ºC

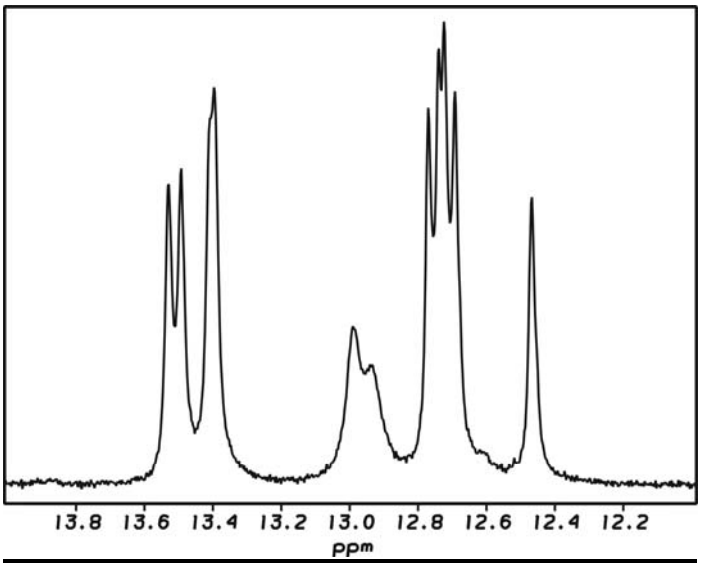

Figure III-5: One-dimensional NMR spectrum of temperature dependence experiment in 10% D_2O/ 90% H_2O, 25 mM NaH_2PO_4, 0.5 mM EDTA, 50mM NaCl buffer, pH 6.78, at 10°C

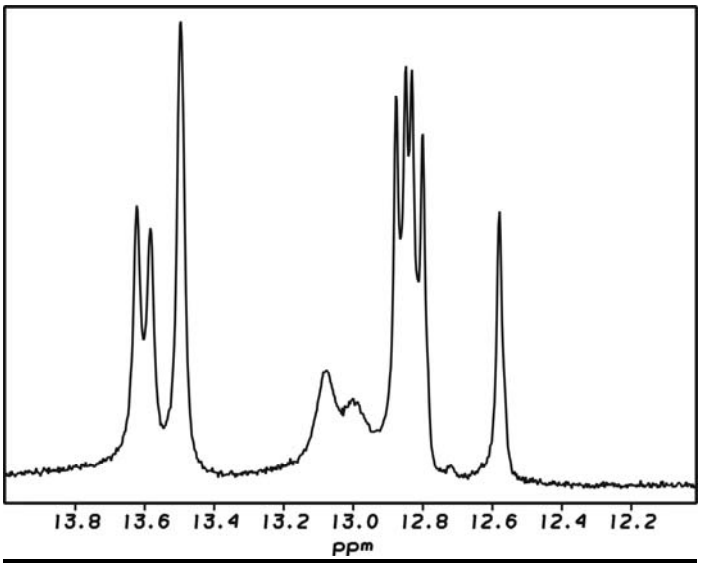

Figure III-6: One-dimensional NMR spectrum of temperature dependence experiment in 10% D_2O/ 90% H_2O, 25 mM NaH_2PO_4, 0.5 mM EDTA, 50mM NaCl buffer, pH 6.78, at 15°C

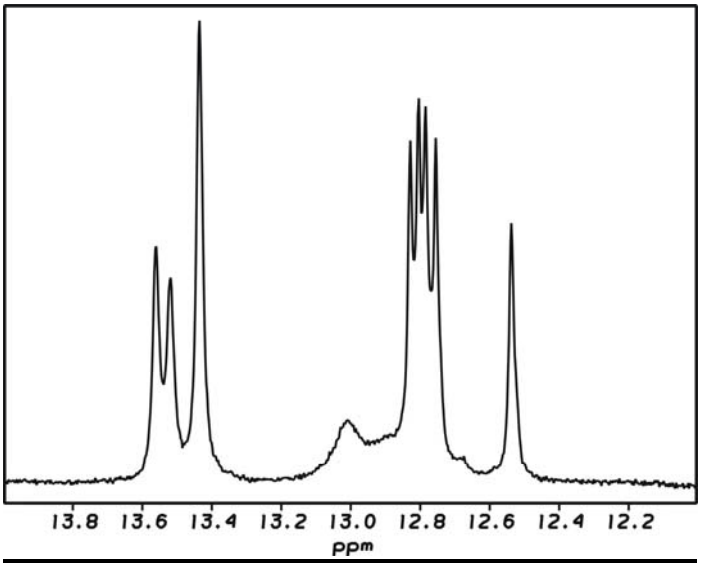

Figure III-7: One-dimensional NMR spectrum of temperature dependence experiment in 10% D_2O/ 90% H_2O, 25 mM NaH_2PO_4, 0.5 mM EDTA, 50mM NaCl buffer, pH 6.78, at 20ºC

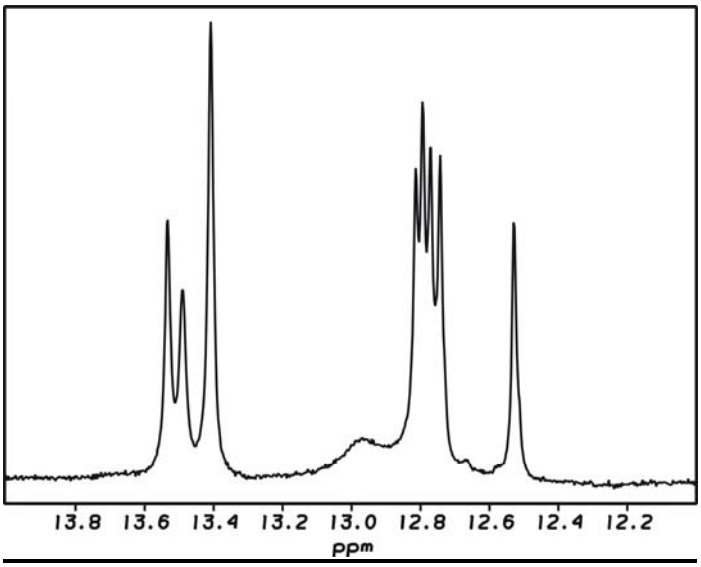

Figure III-8: One-dimensional NMR spectrum of temperature dependence experiment in 10% D_2O/ 90% H_2O, 25 mM NaH_2PO_4, 0.5 mM EDTA, 50mM NaCl buffer, pH 6.78, at 25ºC

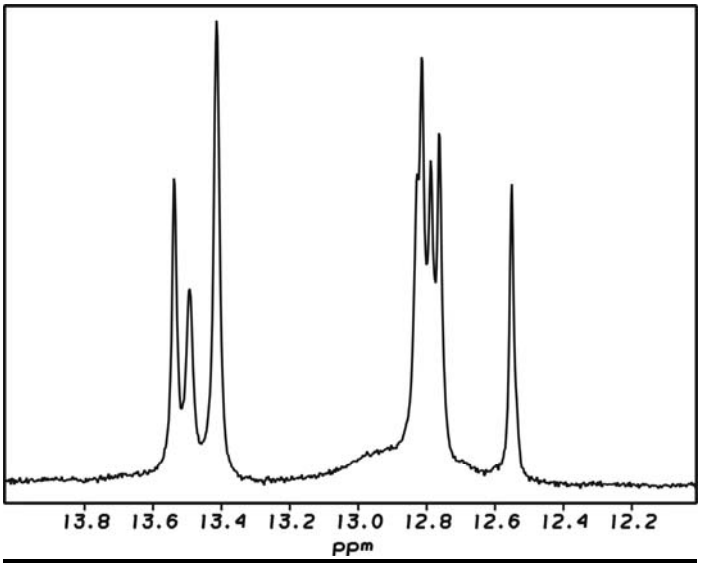

Figure III-9: One-dimensional NMR spectrum of temperature dependence experiment in 10% D_2O/ 90% H_2O, 25 mM NaH_2PO_4, 0.5 mM EDTA, 50mM NaCl buffer, pH 6.78, at 30ºC

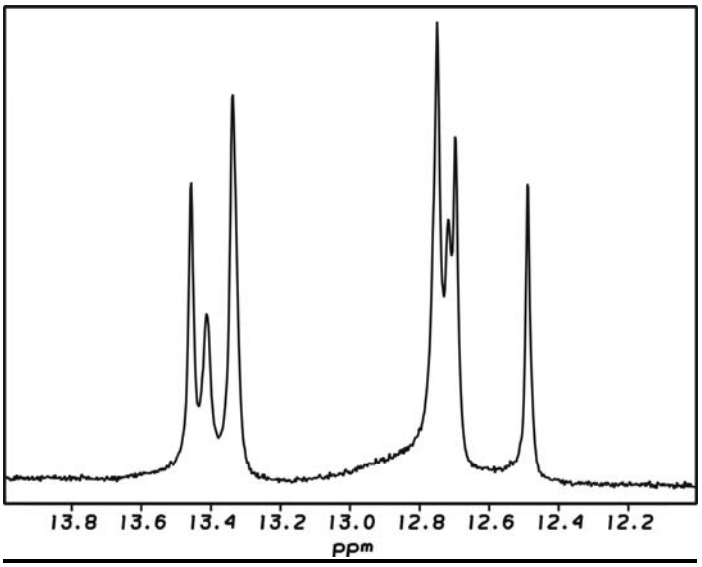

Figure III-10: One-dimensional NMR spectrum of temperature dependence experiment in 10% D_2O/ 90% H_2O, 25 mM NaH_2PO_4, 0.5 mM EDTA, 50mM NaCl buffer, pH 6.78, at 35ºC

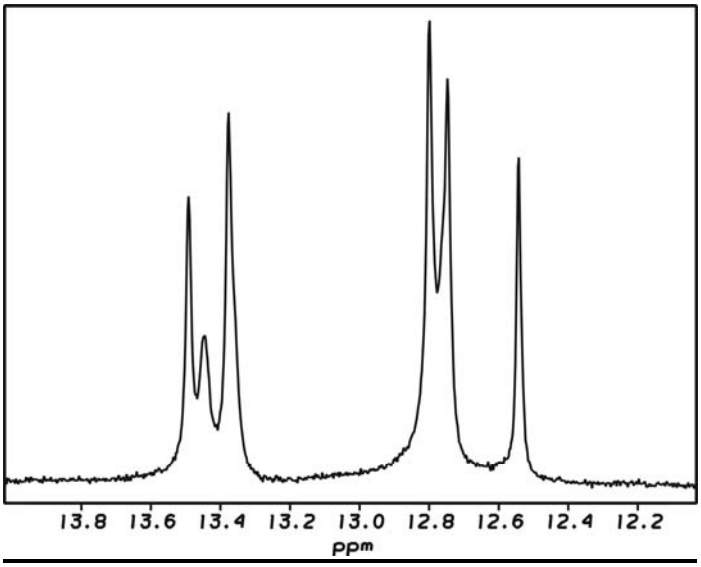

Figure III-11: One-dimensional NMR spectrum of temperature dependence experiment in 10% D_2O/ 90% H_2O, 25 mM NaH_2PO_4, 0.5 mM EDTA, 50mM NaCl buffer, pH 6.78, at 40ºC

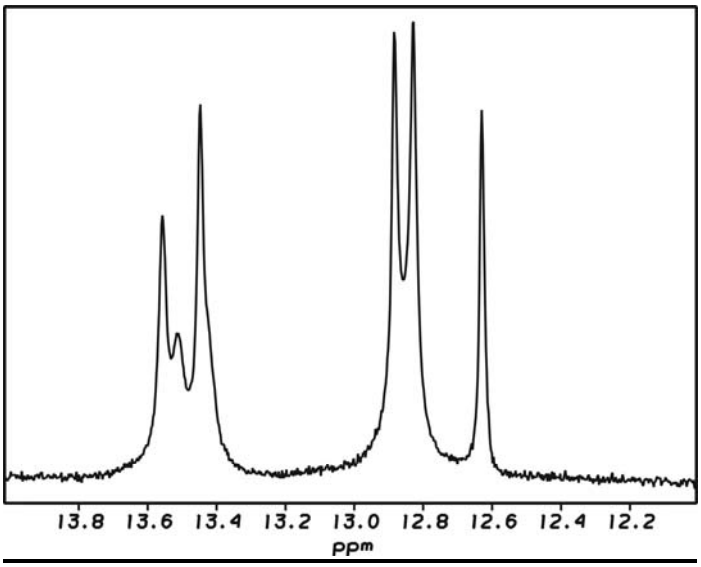

Figure III-12: One-dimensional NMR spectrum of temperature dependence experiment in 10% D_2O/ 90% H_2O, 25 mM NaH_2PO_4, 0.5 mM EDTA, 50mM NaCl buffer, pH 6.78, at 45ºC

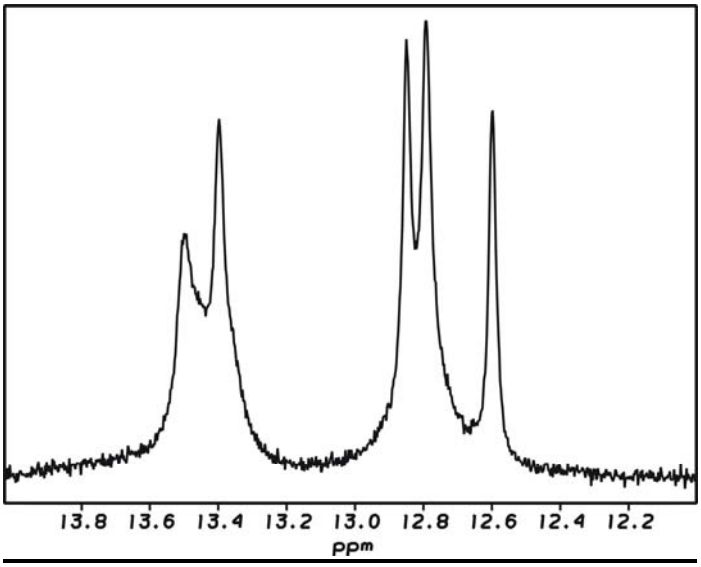

Figure III-13: One-dimensional NMR spectrum of temperature dependence experiment in 10% D_2O/ 90% H_2O, 25 mM NaH_2PO_4, 0.5 mM EDTA, 50mM NaCl buffer, pH 6.78, at 50°C

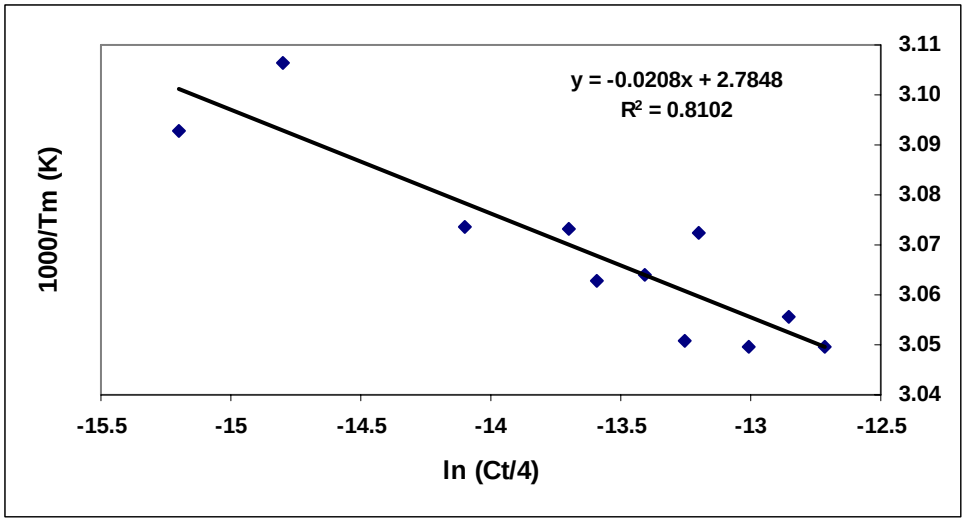

Figure III-14: Graph of reciprocal melting temperature versus ln(Ct/4).

$\Delta H°$ (kcal/mol)	$\Delta S°$ (kcal/mol*K)	$\Delta G^{\circ}_{25°C}$ (kcal/mol)	$\Delta G^{\circ}_{37°C}$ (kcal/mol)
-95.5	**-.267**	**-15.9**	**-12.7**

Table II: Thermodynamic parameters determined for unmodified 11-mer duplex.

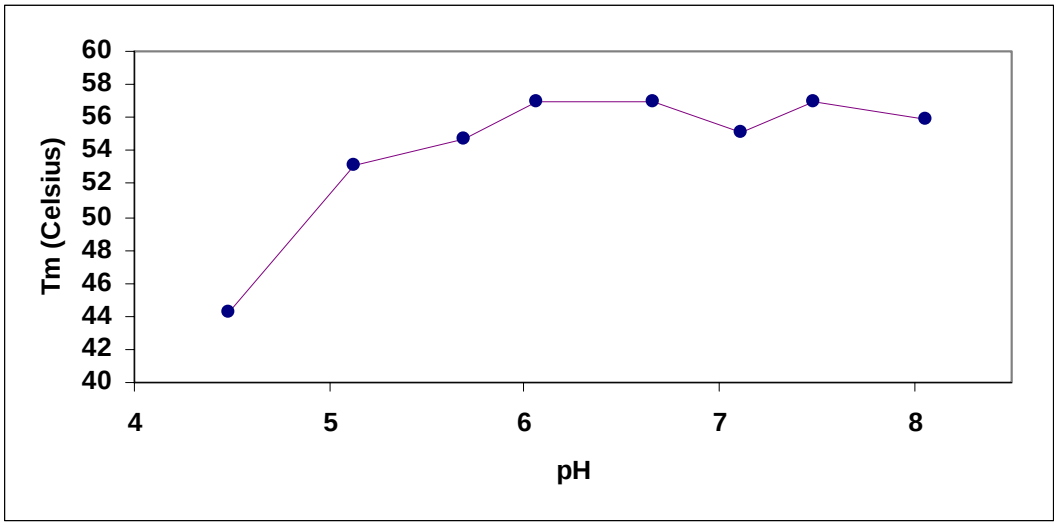

Figure III-15: Graph of Tm measured at varying pH of the unmodified 11-mer duplex.

11-mer duplex containing 3-ABA

The two dimensional ^{1}H NOESY spectrum of the 11-mer containing 3-ABA performed in 100% D_2O buffer is presented in figure III-16. Upon closer inspection of the base-H1' region (figure III-19) there appears to be a doubling of peaks that at first indicates the presence of two conformations of duplex DNA. As shown in the figure, upon performance of the NOE walk, a pivotal, initial step in resonance assignment, there is displayed two peaks for guanine in the second position and cytosine in the fifth position of the duplex sequence. Qualitative inspection of the full spectrum revealed doubling of peaks throughout. Therefore the sample was subjected to more testing.

As presented in figure III-21, melting experiments were performed to calculate the Tm of the samples and extract other thermodynamic information. The figure presents the melting stability of the unmodified 11mer duplex and the 11mer duplex containing the 3-ABA adduct. It appears that the duplex containing the 3-ABA destabilizes DNA causing it to have a lower T_m. However, the reliability of this data is uncertain as there may have been more than one structure present in the solution containing the damaged duplex.

A one dimensional spectrum of the sample was taken in H_2O buffer, revealing that there appeared to be more than one conformation of the duplex DNA in the sample. Also, exchange protons were observed in the H1' deoxyribose sugar proton region as indicated by red arrows in figure III-20, signifying the presence of multiple conformations. However, upon inspection of the mass spectrometric data (figure III-17 and III-18) there appeared to be the presence of a highly pure substance.

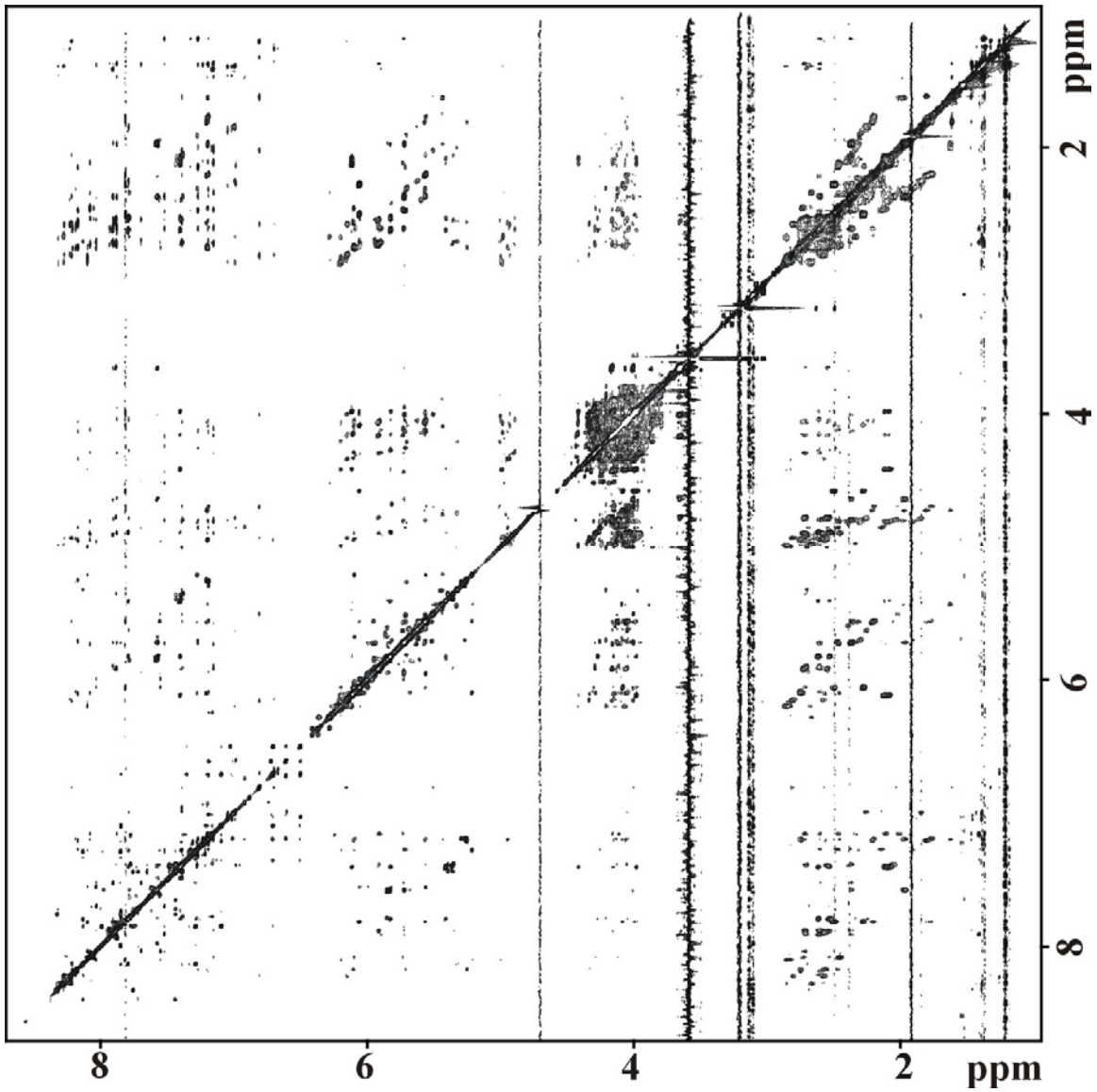

Figure III-16: ^{1}H NOESY spectrum of 11-mer duplex containing 3-ABA recorded in 100% D_2O buffer, 25 mM NaH_2PO_4, 0.5 mM EDTA, 50mM NaCl buffer, pH 6.8, 25^o C, at 350 ms mixing time.

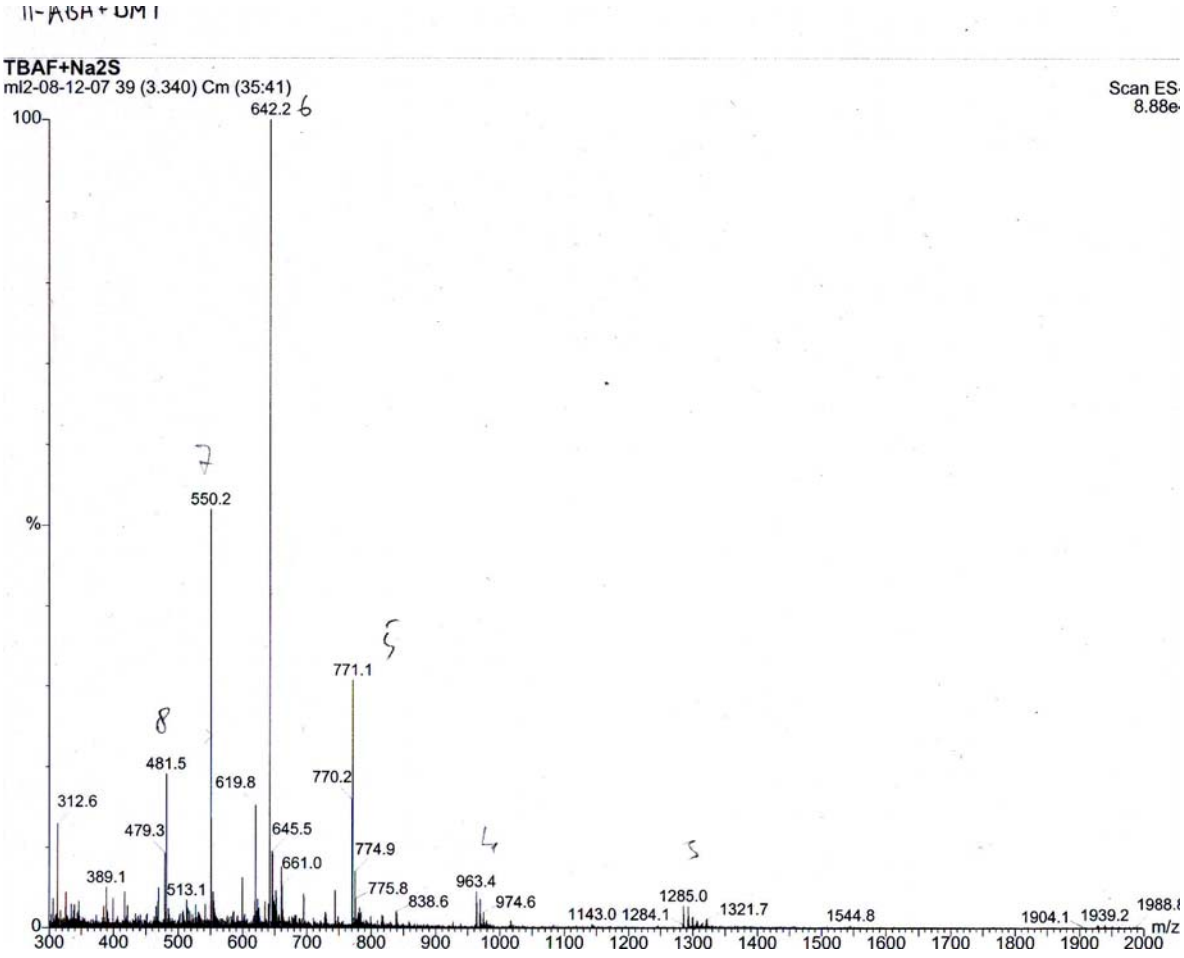

Figure III-17: Electrospray ionization mass spectrum of 11-mer duplex containing 3-ABA and the DMT (dimethoxytrityl) group.

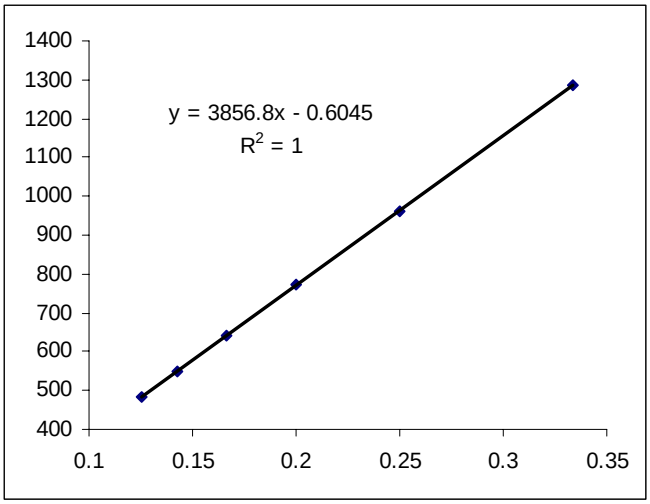

Figure III-18: Graph of ESI-MS data with calculated molecular mass of 11-mer duplex containing 3-ABA and DMT group of 3856 g/mol.

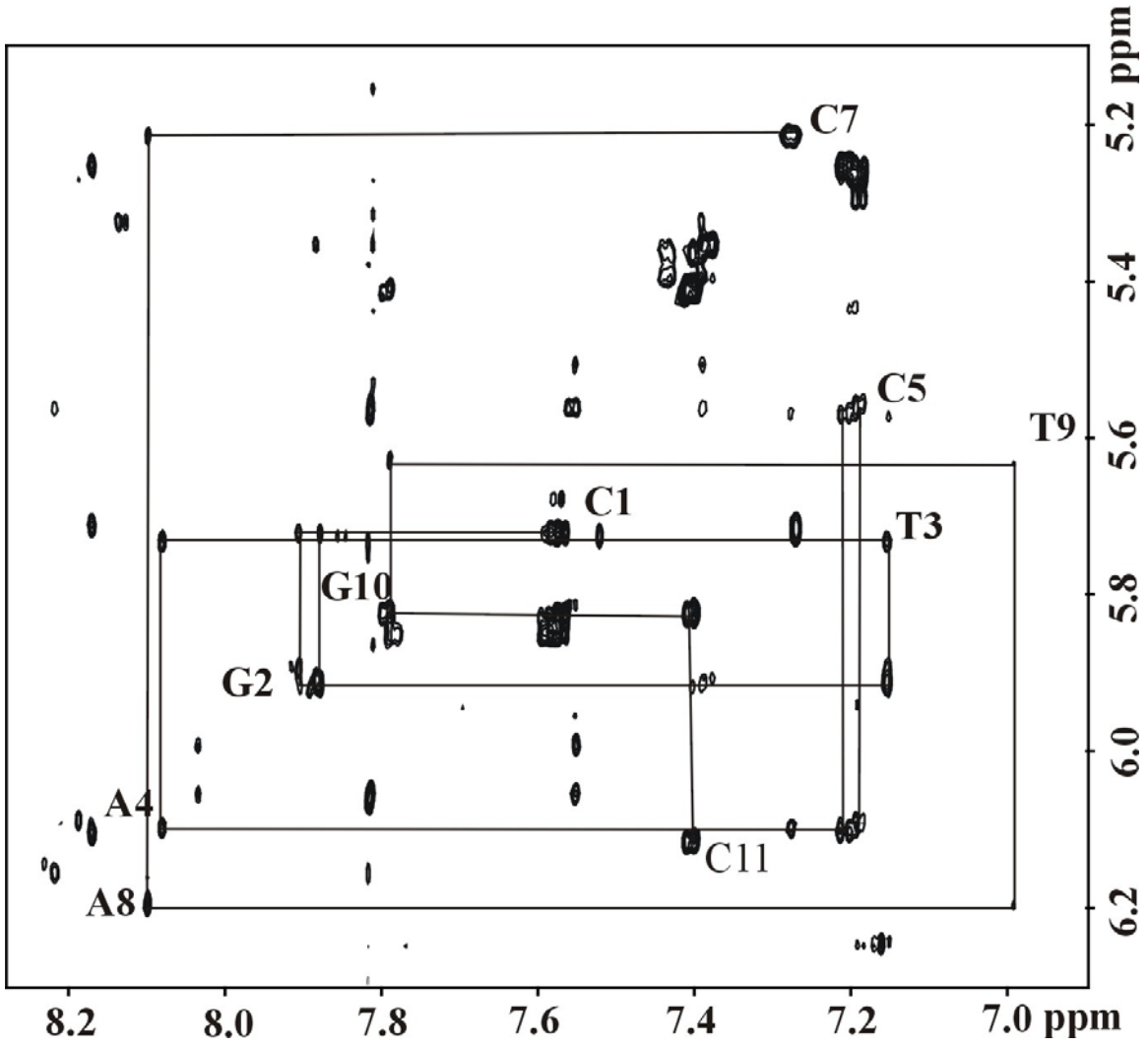

Figure III-19: Contour plot of NOESY spectrum of 11-mer duplex containing 3-ABA recorded in 100% D_2O buffer, pH = 6.8, 25° C, 350 ms mixing time. Plot displays region containing base (H8 of purines and H6 of pyrimidines) and H1' deoxyribose sugar protons.

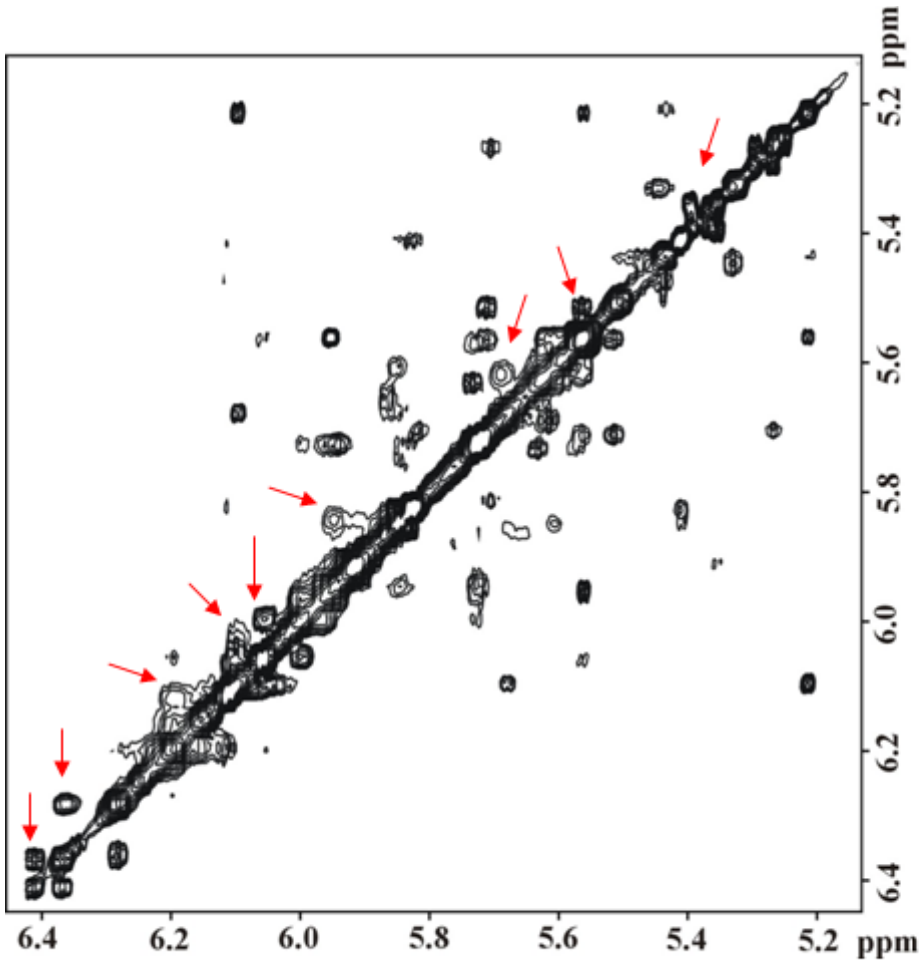

Figure III-20: Contour plot of NOESY spectrum of 11-mer duplex containing 3-ABA recorded in 100% D_2O buffer, pH = 6.8, 25° C at 350 ms mixing time. Plot displays region containing H1' deoxyribose sugar protons. Red arrows designates exchange protons.

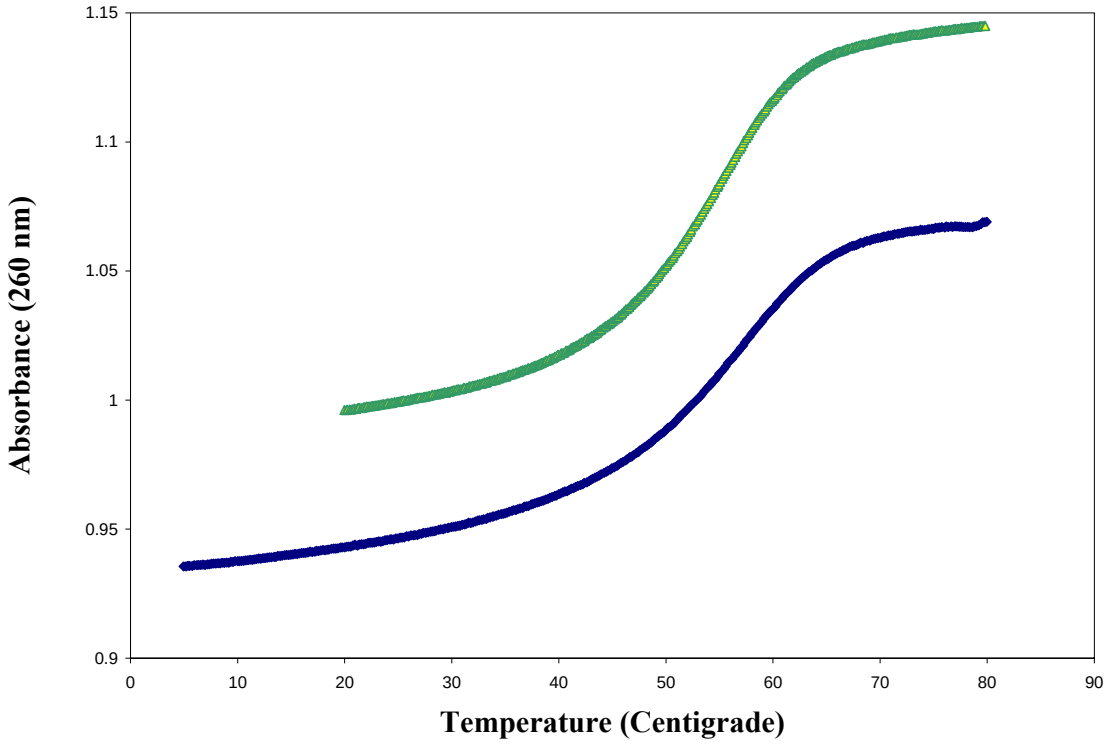

Figure III-21: Thermal dependence data for the unmodified 11-mer duplex (green) and the 11-mer duplex containing 3-ABA (blue) recorded in 200mM NaCl buffer containing 0.5mM EDTA at a pH of 6.8.

Unmodified 14-mer duplex

The two dimensional ^{1}H NOESY spectrum of the unmodified 14-mer duplex containing 3-ABA performed in 100% D_2O buffer is presented in figure III-22. Upon inspection of the base-H1' region (figure III-23), some overlaps were found between C6 and C7 protons. Chemical shift values for non-exchangeable protons are presented in table III.

Thermodynamic parameters of the oligonucleotide duplex were extracted from the melting experiments of the oligonucleotide strands performed at varying concentrations as displayed in table V.

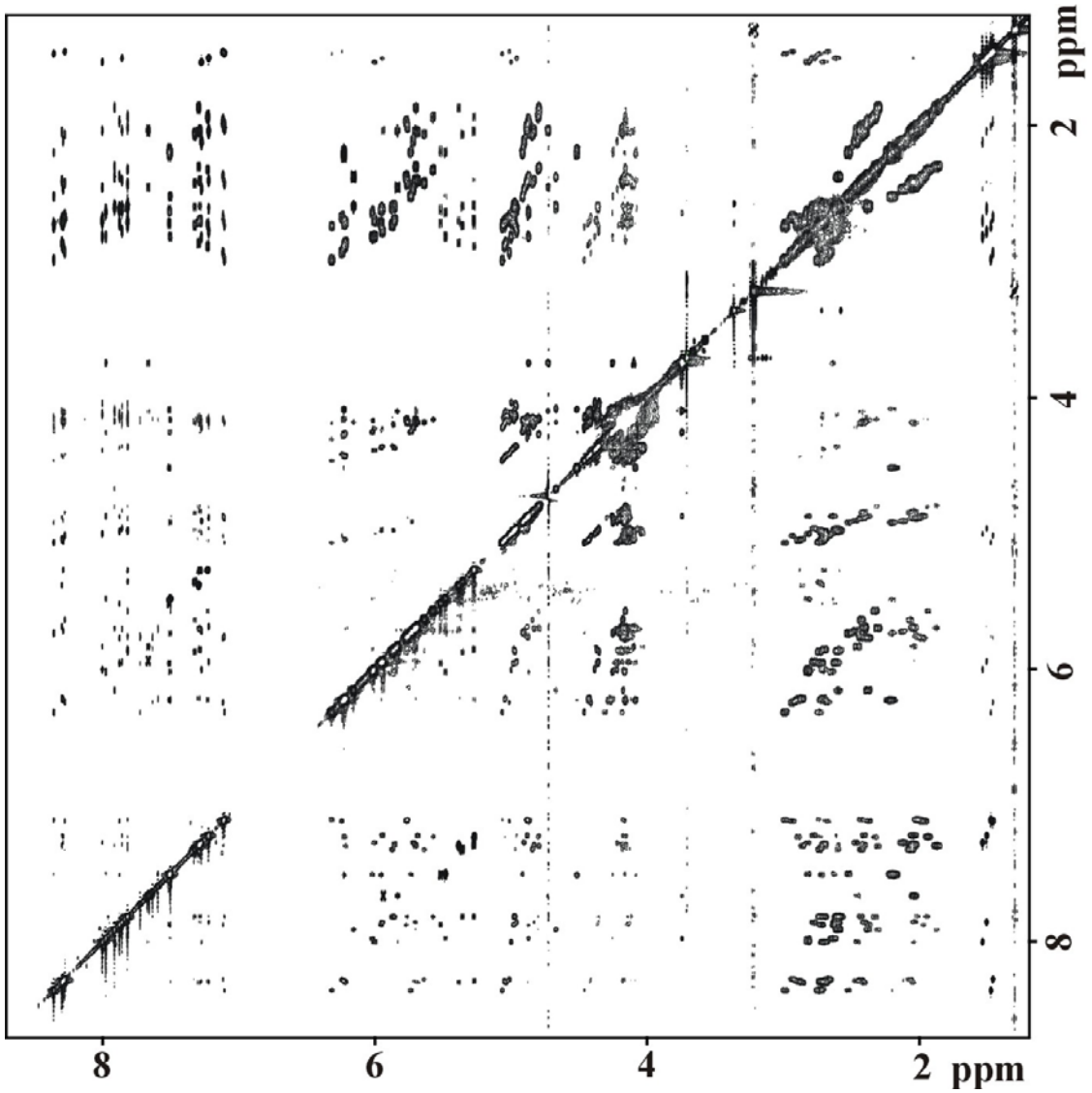

Figure III-22: ^{1}H NOESY spectrum of unmodified 14-mer duplex recorded in 100% D_2O buffer, 25 mM NaH_2PO_4, 0.5 mM EDTA, 50mM NaCl buffer, pH 6.8, 25^{o} C, at 300 ms mixing time.

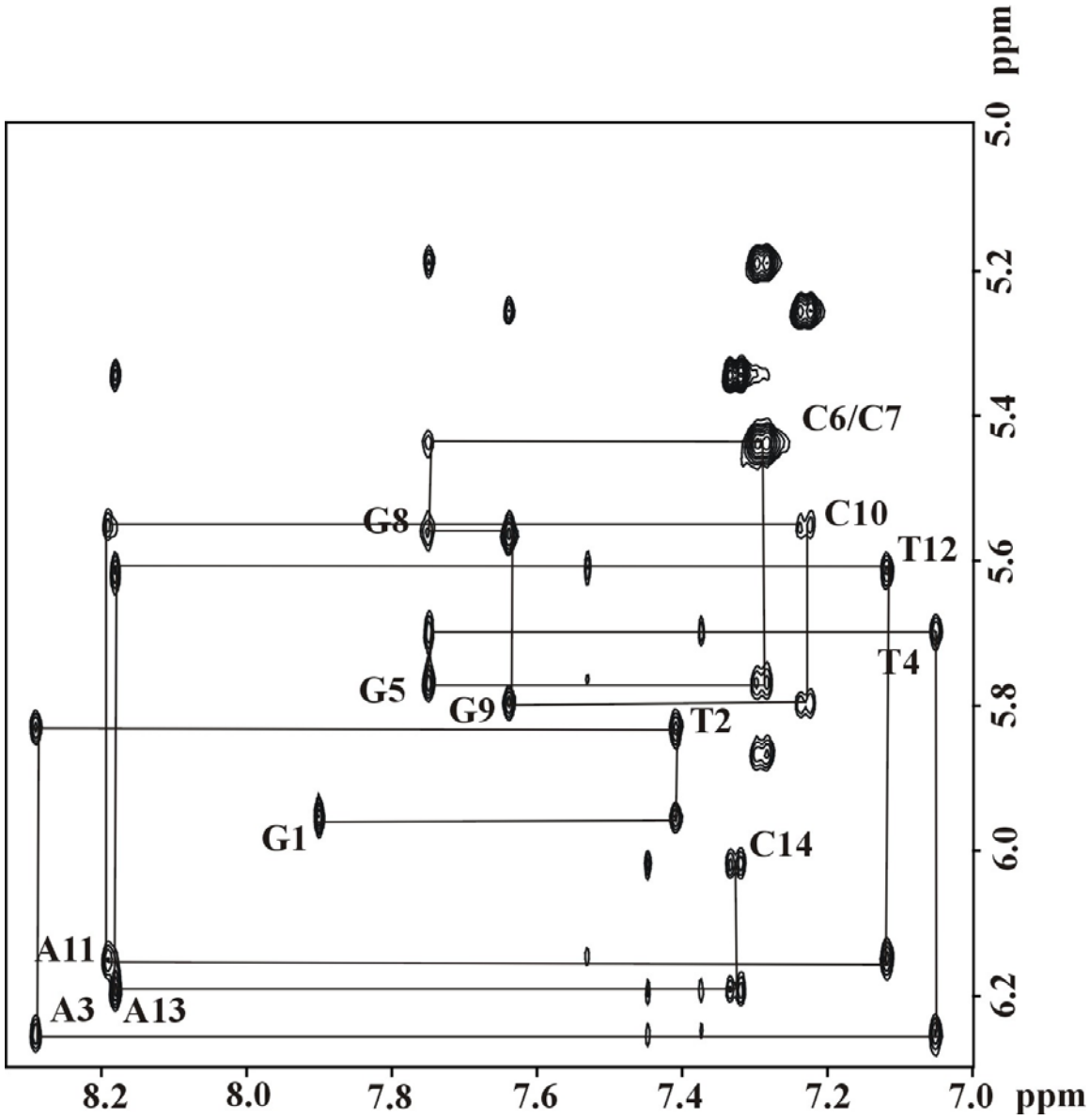

Figure III-23: Contour plot of NOESY spectrum of the unmodified 14-mer duplex recorded in 100% D_2O buffer, pH = 6.8, 25° C, 300 ms mixing time. Plot displays region containing base (H8 of purines and H6 of pyrimidines) and H1' deoxyribose sugar protons.

Base	H1'	H2'	H2''	H3'	H4'	H6 H8	CH3 H5 H2
G1	5.95	2.63	2.73	N/A	N/A	7.90	N/A
T2	5.83	2.24	2.56	4.89	N/A	7.41	1.37
A3	6.25	2.64	2.91	4.98	N/A	8.29	N/A
T4	5.70	1.95	2.37	N/A	N/A	7.05	1.35
G5	5.77	2.53	2.59	4.90	N/A	7.75	N/A
C6	5.87	N/A	2.59	N/A	N/A	7.29	5.19
C7	5.44	N/A	N/A	N/A	N/A	7.29	5.44
G8	5.56	2.60	2.68	N/A	N/A	7.75	N/A
G9	5.80	2.47	2.65	4.90	N/A	7.64	N/A
C10	5.55	1.99	2.34	N/A	N/A	7.23	5.25
A11	6.15	2.59	2.84	N/A	N/A	8.20	N/A
T12	5.61	1.94	2.33	4.91	N/A	7.12	1.41
A13	6.19	2.58	2.79	4.94	N/A	8.18	N/A
C14	6.02	2.03	2.07	N/A	N/A	7.33	5.34

Table III: Chemical shift values for unmodified 14-mer duplex measured at 25ºC. Chemical shifts are referenced to TSP. N/A: not assigned.

14-mer duplex containing 3-ABA

The two dimensional ^{1}H NOESY spectrum of 14-mer duplex containing 3-ABA performed in 100% D_2O buffer is presented in figure III-24. Upon inspection of the base-H1' region (figure III-24) a number of overlaps can be seen in the base-H1' region including the following: G1 H8 / G5 H8; C6 H1' / C7 H5; G8 H1' / C14 H5; G9 H1' / C10 H5; C10 H1' / C10 H5; A11 H8 / A13 H8. Chemical shift values for non-exchangeable protons are presented in table IV. Assignment of 3-ABA protons was facilitated by data obtained from NOESY, DQF-COSY and TOCSY90 spectra (figures III-25 to 27) and is also presented in table IV.

NOE interactions can be seen between the benzanthrone protons and that of the preceding base, thymine on the 4th position of the duplex sequence in figures III-25 to III-27 implying that 3-ABA adduct is directed towards the 5'-end of the duplex.

With the help of Ms. Tanya Zaliznyak, melting curves for the unmodified 14-mer duplex and 14-mer duplex containing 3-ABA were generated. The graph of reciprocal melting temperature versus ln(Ct/4) is shown in figure III-29. Upon inspection, it appears that the 3-ABA lesion stabilizes the duplex causing it to have a higher T_m. This data implies that 3-ABA adduct may be helix-stabilizing.

Thermodynamic parameters of the oligonucleotide duplex were extracted from the melting experiments of the oligonucleotide strands performed at various concentrations. From a plot of $1000/T_m$ versus ln (Ct/4), $\Delta G^{\circ}_{25^{\circ}C}$ = -19.7 kcal/mol, and $\Delta G^{\circ}_{37^{\circ}C}$ = -16.8

kcal/mol for the 14-mer duplex containing 3-ABA as compared to $\Delta G^{\circ}_{25^{\circ}C}$ = -18.0 kcal/mol, and $\Delta G^{\circ}_{37^{\circ}C}$ = -14.8 kcal/mol for the unmodified 14-mer duplex. The lower free energy of the 14-mer duplex containing 3-ABA implies an increase in stability as compared to the unmodified duplex.

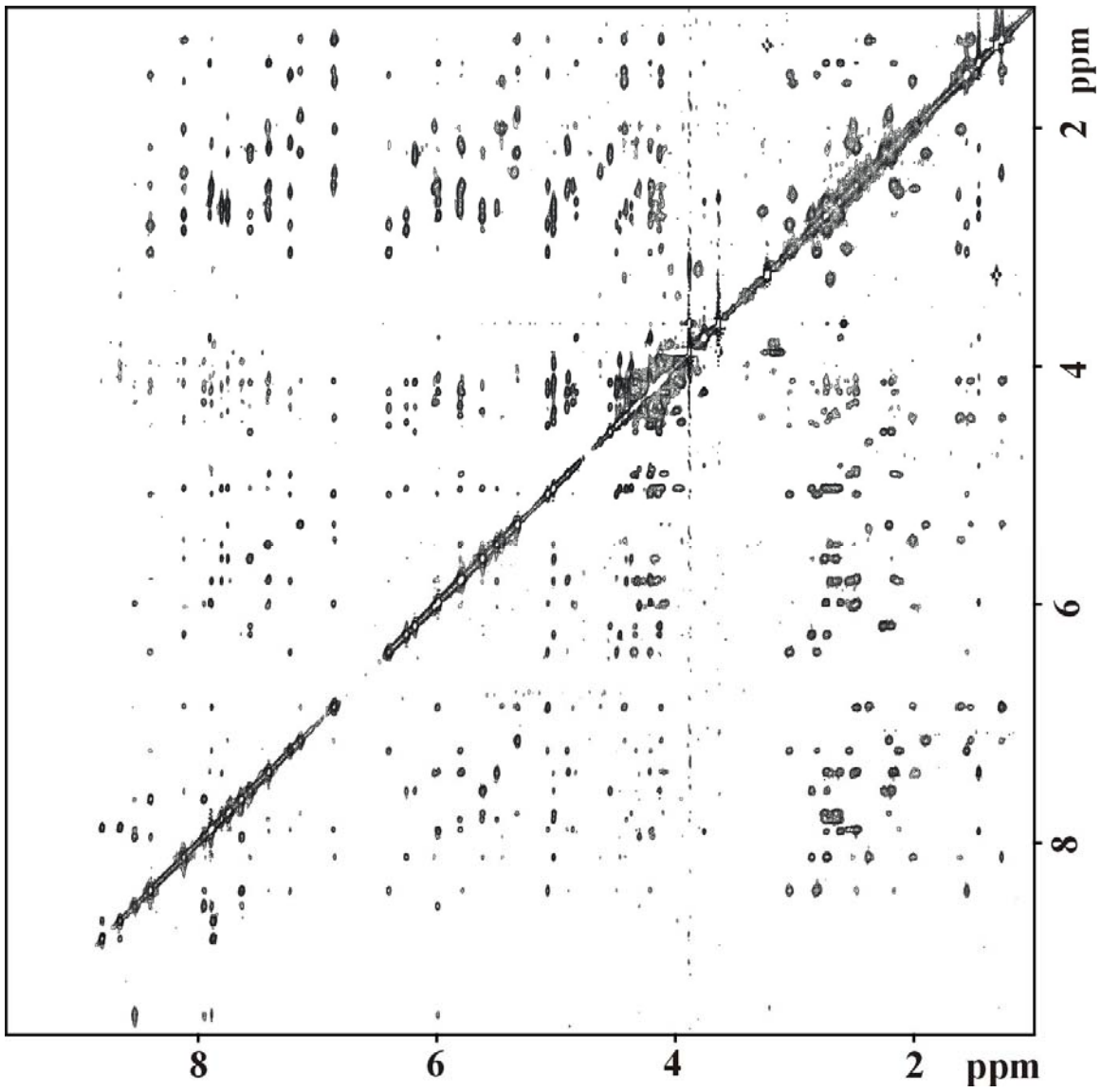

Figure III-24: ^{1}H NOESY spectrum of 14-mer duplex containing 3-ABA recorded in 100% D_2O buffer, 25 mM NaH_2PO_4, 0.5 mM EDTA, 50mM NaCl buffer, pH 6.8, 25° C, at 300 ms mixing time.

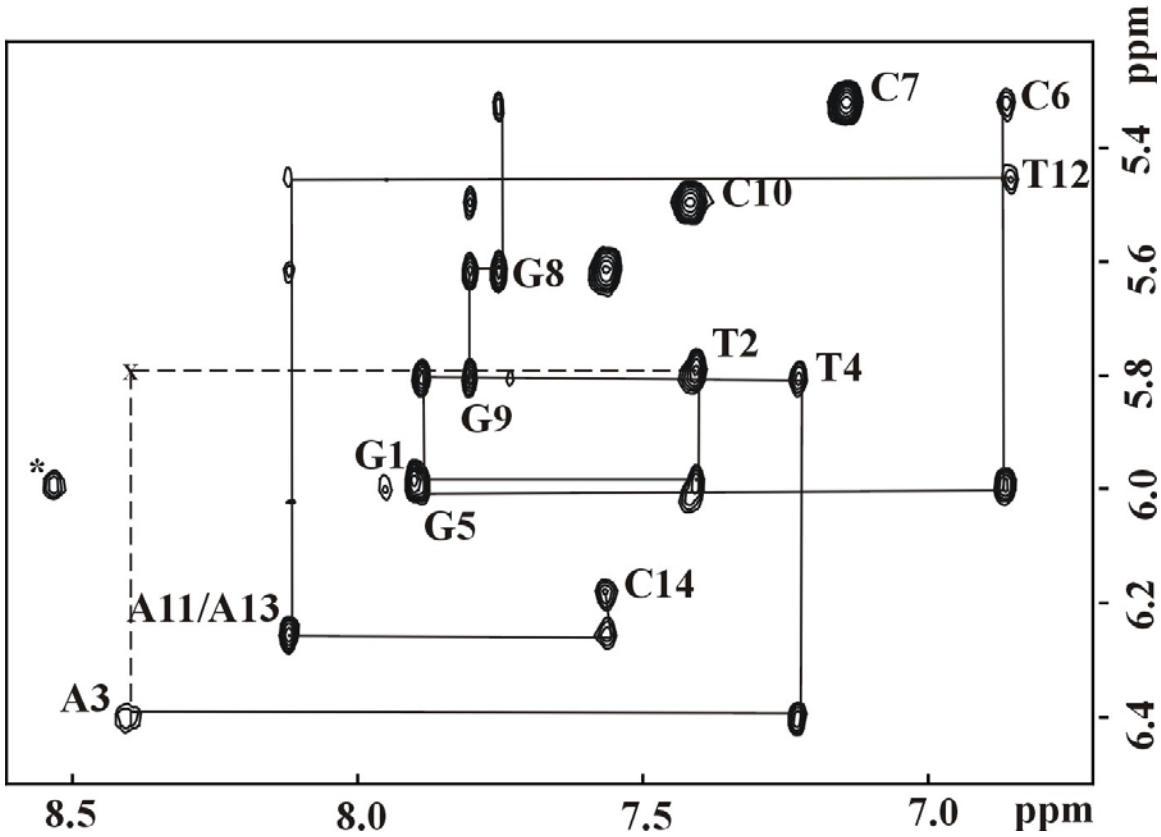

Figure III-25: Contour plot of NOESY spectrum of 14-mer duplex containing 3-ABA recorded in 100% D_2O buffer, 25 mM NaH_2PO_4, 0.5 mM EDTA, 50mM NaCl buffer, pH 6.8, 25° C, 300 ms mixing time. Plot displays region containing base (H8 of purines and H6 of pyrimidines) and H1' deoxyribose sugar protons. X represents missing peak; * represents NOE cross peak between 3-ABA proton H11 proton and G5 H1' proton.

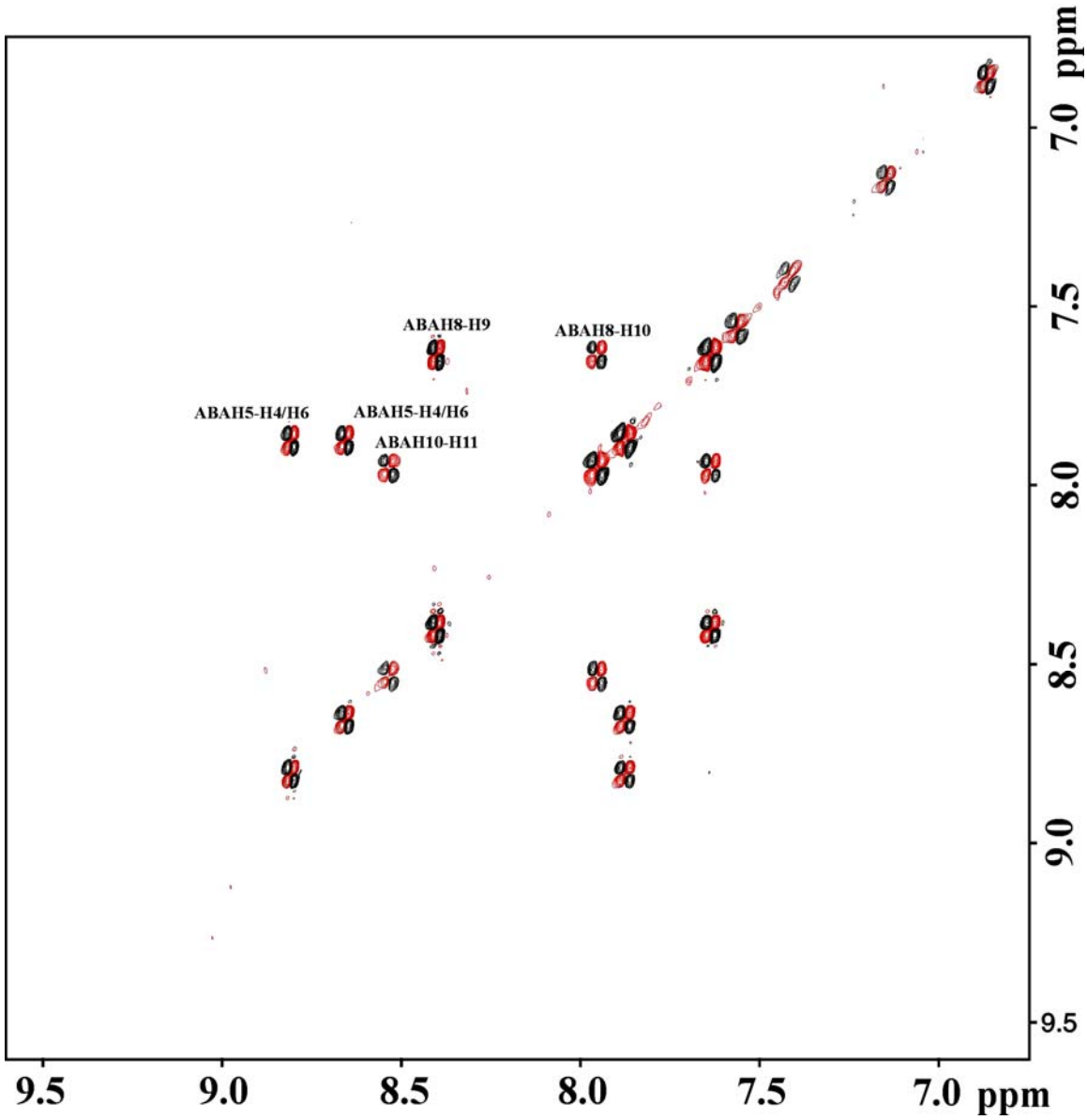

Figure III-26: Contour plot of DQF-COSY spectrum of 14-mer duplex containing 3-ABA recorded in 100% D_2O buffer, 25 mM NaH_2PO_4, 0.5 mM EDTA, 50mM NaCl buffer, pH 6.8, at 25° C. Plot displays region containing partially labeled 3-ABA protons.

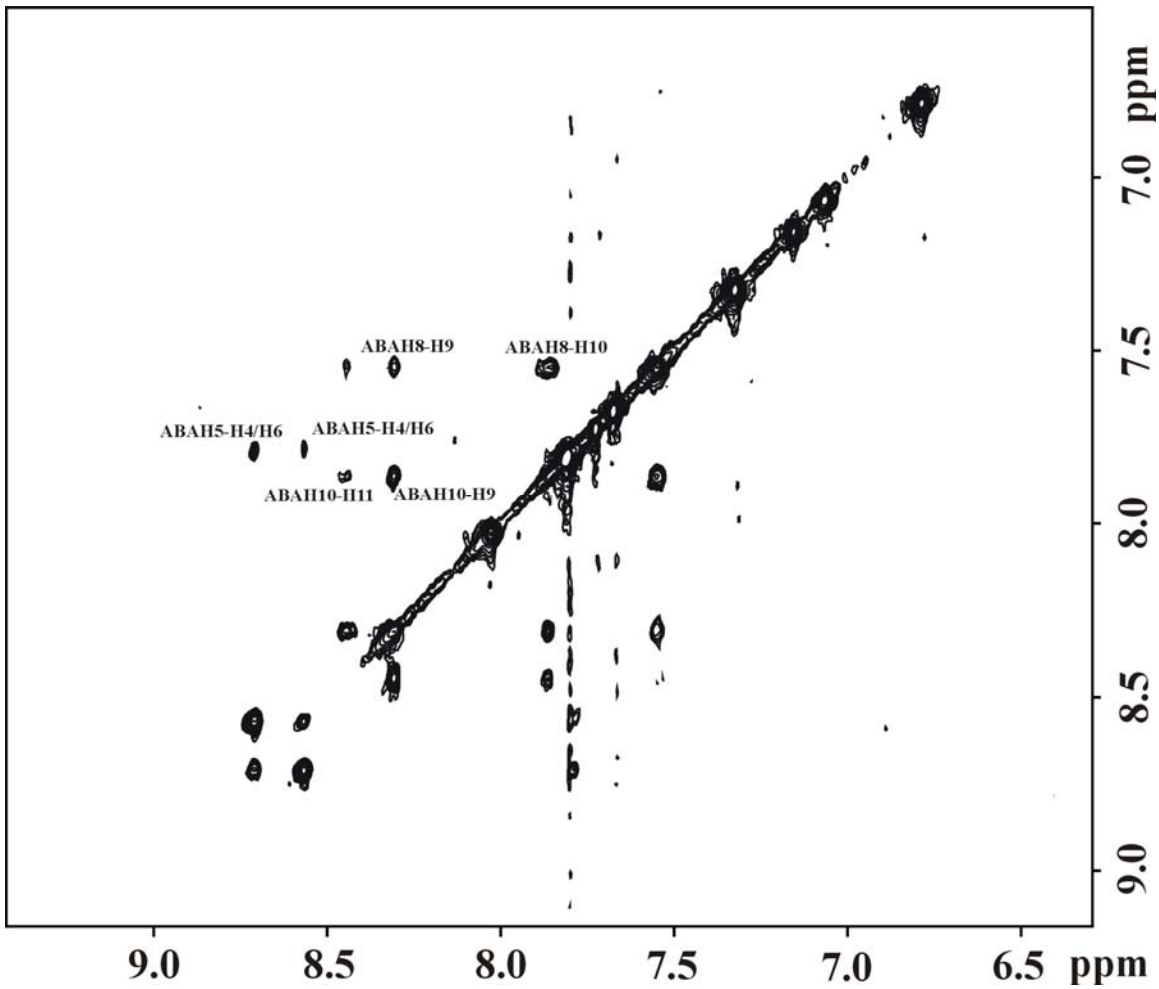

Figure III-27: Contour plot of TOCSY spectrum of 14-mer duplex containing 3-ABA recorded in 100% D_2O buffer, pH = 6.8, 25° C at 90 ms mixing time. Plot displays region containing partially labeled 3-ABA protons.

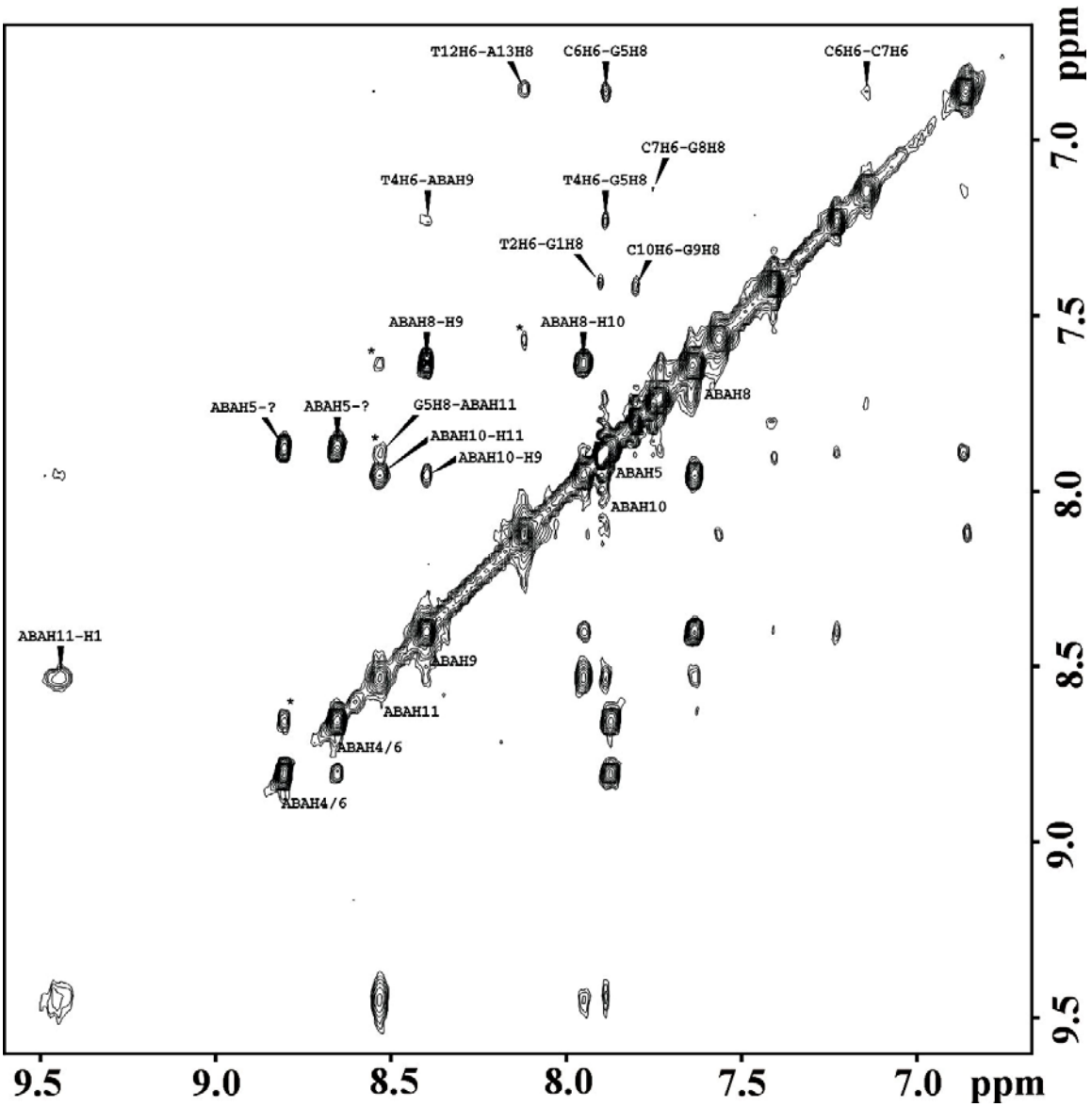

Figure III-28: Contour plot of NOESY spectrum of 14-mer duplex containing 3-ABA recorded in 100% D_2O buffer, 25 mM NaH_2PO_4, 0.5 mM EDTA, 50mM NaCl buffer, pH 6.8, 25° C, 300 ms mixing time. Plot displays region containing labeled base (H8 of purines and H6 of pyrimidines) and 3-ABA protons.

Base	H1’	H2’	H2’’	H3’	H6 H8	CH3 H5 H2
G1	5.99	2.62	2.7	N/A	7.90	N/A
T2	5.79	2.16	2.48	4.90	7.41	1.46
A3	6.40	2.81	3.04	5.07	8.40	N/A
T4	5.81	2.12	2.54	4.91	7.23	1.56
G5	5.99	N/A	N/A	5.07	7.89	N/A
C6	5.32	1.26	1.53	N/A	6.86	5.07
C7	5.32	1.90	2.21	N/A	7.14	5.3
G8	5.62	2.65	2.75	5.02	7.75	N/A
G9	5.80	N/A	N/A	5.02	7.80	N/A
C10	6.01	N/A	N/A	N/A	7.42	5.50
A11	N/A	2.01	2.38	N/A	8.12	N/A
T12	5.45	1.26	1.61	N/A	6.86	1.26
A13	6.25	2.73	2.86	N/A	8.12	N/A
C14	6.18	2.19	2.25	5.02	7.56	5.62

ABA moiety	H4/H6	H5	H8	H9	H10	H11	H1
G5*	8.65/8.80	7.87	7.63	8.40	7.95	8.53	9.44

Table IV: Chemical shift values for 14-mer duplex containing 3-ABA adduct measured at 25ºC. Chemical shifts are referenced to TSP. N/A: not assigned.

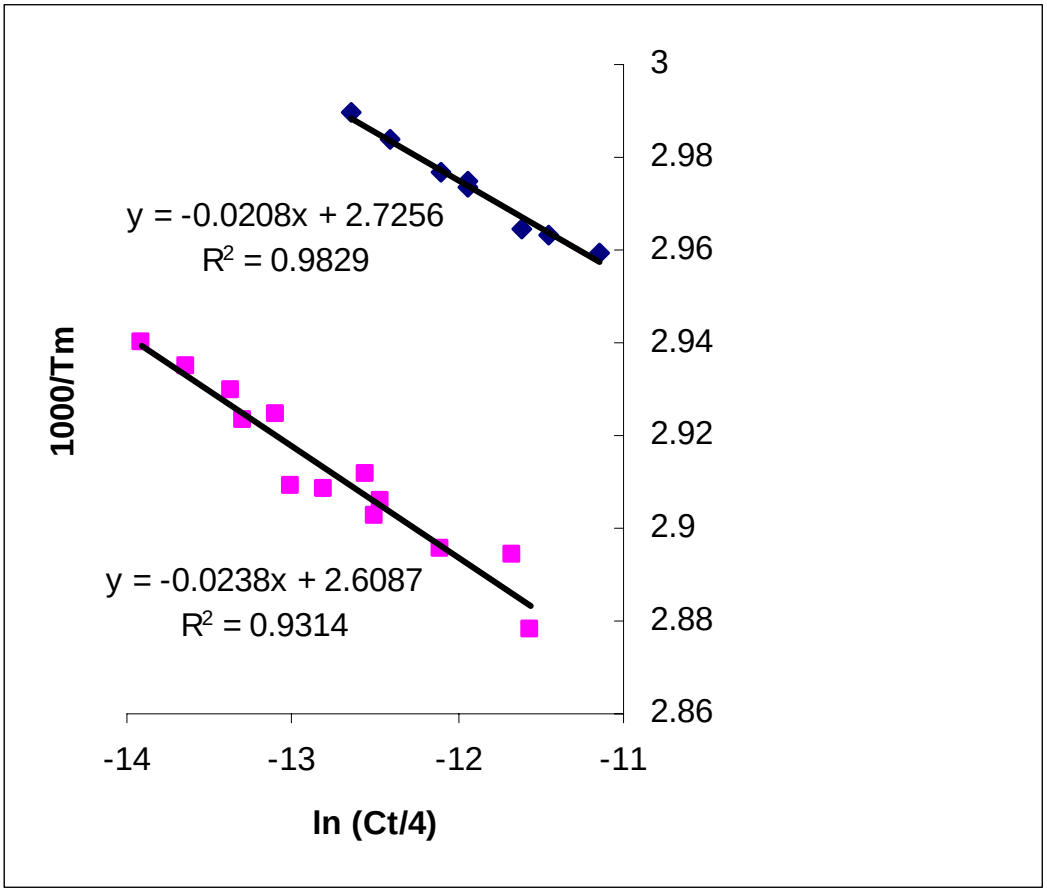

Figure III-29: Reciprocal melting temperature vs. ln (C_t/4) plot for unmodified 14-mer duplex (blue squares) and 14-mer duplex containing 3-ABA (pink squares.)

ΔH° (kcal/mol)	ΔS° (kcal/mol K)	$\Delta G°_{25°C}$ (kcal/mol)	$\Delta G°_{37°C}$ (kcal/mol)
-95.7	**-0.261**	**-18.0**	**-14.8**

Table V: Thermodynamic parameters determined for the unmodified 14-mer duplex.

ΔH° (kcal/mol)	ΔS° (kcal/mol K)	$\Delta G°_{25°C}$ (kcal/mol)	$\Delta G°_{37°C}$ (kcal/mol)
-91.6	**-0.241**	**-19.7**	**-16.8**

Table VI: Thermodynamic parameters determined for the 14-mer duplex containing 3-ABA.

Discussion

Structural characterization of the unmodified 11-mer duplex was successfully accomplished. However, initial NOESY spectra of the same 11-mer duplex containing 3-ABA proved challenging. There appeared to be a doubling of peaks throughout the NOESY spectrum implying the presence of more than one structure in solution. There was concern as to whether this was a result of the 3-ABA lesion inherently causing the doubling due to its destabilizing nature or whether the duplex sequence chosen precluded the correct adoption of the lesion in the duplex. Also, the duplex may not have been properly annealed causing the spectra to be ambiguous. Therefore, a new sequence was generated for further investigation.

The new sequence generated was self-complementary for the reason that it would allow easier resonance assignment and synthesis. Additionally, because it was unclear whether the 3-ABA adduct would be directed towards the 5'- or 3'- end of the duplex DNA, the length of the oligonucleotide was extended from an 11-mer to a 14-mer and the lesion placed on the guanine in the 5^{th} position of the sequence thereby separating the two lesions on the duplex by four base pairs. This separation would prevent any hindrance that may have resulted from the proximity of the two lesions.

From the 1D spectrum of the unmodified 14-mer duplex, it was clear that only one structure was found in solution. However, a number of peaks were found to overlap in the NOESY spectrum of the unmodified 14-mer duplex.

The issue with peaks overlapping was more apparent upon inspection of the NOESY spectrum obtained of the 14-mer duplex containing 3-ABA. Additionally, 3-ABA was found to be directed toward the 5' end of duplex DNA based on NOE interactions between protons on the lesion and the preceding base in the duplex sequence, thymine in the 4^{th} position. New experiments were determined to be needed in order to resolve the issue of peak overlaps and avoid ambiguities with resonance assignment.

Preliminary data from melting curve experiments suggests that 3-ABA is a helix-stabilizing lesion which is crucial step towards development of the theory behind NER mechanism recognition and may potentially explain why in some studies the 3-ABA adduct escapes DNA damage repair.

Conclusions and Future work

Certainly, 3-nitrobenzanthrone is a compound that deserves further investigation; furthermore, identifying the structural changes that it affects in DNA will aid in the understanding of its mechanism. Spectroscopic methods complemented with computational studies offers an efficient method in identifying the structure of 3-nitrobenzanthrone incorporated into an oligonucleotide. Already, hundreds of nucleic acid structures have been solved using NMR spectroscopy as it offers several advantages to other structure determination methods. The results of this structural identification may prove to offer some insight into the NER mechanism of recognition.

One of the major challenges to overcome in these experiments is the peak overlaps found in the spectra of both the unmodified 14-mer duplex and the 14-mer duplex containing 3-ABA. Overlapping makes structure determination difficult as it is uncertain how to correctly assign proton resonances. One way to resolve the overlaps that are displayed in the spectra of the duplex DNA is to reduce the number of base pairs separating the two lesions. Originally, a fourteen base-pair self-complementary sequence was chosen in order to avoid hindrance between the moieties in the event there was contact between them because it was unknown what orientation the lesions would have within the duplex. However, from the NOESY spectrum of the 14-mer duplex containing 3-ABA it was determined that the 3-aminobenzanthrone lesion is directed towards the 5' end due to NOE interactions that can be seen between the benzanthrone protons and that of the preceding base on the 5' end of the duplex. Therefore, it may be possible to reduce the overlaps seen in the 14mer duplex DNA spectrum by reducing the number of base pairs separating the two lesions. Future experiments would involve synthesizing a self-complementary strand with two or four base pairs removed separating the two 3-ABA lesions.

Another proposed ways to reduce overlap is to work with the original non self-complementary sequence and reduce the number of base pairs by two. Because the 3-aminobenzanthrone is a helix-stabilizing lesion, the shorter sequence is expected to have the stability necessary to generate utilizable results. Even though, it may be advantageous to continue working with self-complementary sequence to make for easier spectra interpretation.

References

1 Enya, T. , Suzuki, H., Watanabe, T., Hirayama, T., Hisamatsu, Y. 3-Nitrobenzanthrone, a Powerful Bacterial Mutagen and Suspected Human Carcinogen Found in Diesel Exhaust and Airborne Particulates. *Environ. Sci. Technol.* **1997**, 31, 2772-2776

2 Poirier M.C., Santella R.M., Weston A. Carcinogen macromolecular adducts and their measurement. *Carcinogenesis*. **2000**, 3, 353-9

3 Gillet, L.C.J, Scharer, O.D. Molecular Mechanisms of Mammalian Global Genome Nucleotide Excision Repair. *Chem. Rev.* **2006**, 106, 253-276

4 Hess, M.T., Schwitter, U., Petretta, M., Giese, B., Naegeli, H. Bipartite substrate discrimination by human nucleotide excision repair. *Proc. Natl. Acad. Sci. USA.***1997**, 94, 6664-6669

5 Geacintov, N.E., Broyde, S., Buterin, T., Naegeli, H., Wu, M., Yan, S. Patel, D.J. Thermodynamic and Structural Factors in the Removal of Bulky DNA Adducts by the Nucleotide Excision Repair Machinery. *Biopolymers.* **2002**, 65, 202-210

6 Zaliznyak, T., Bonala, R., Johnson, F. and de los Santos, CR. Structure and Stability of Duplex DNA Containing the 3-(Deoxyguanosin-*N*2-yl)-2-acetylaminofluorene (dG(*N*2)-AAF) Lesion: A Bulky Adduct that Persists in Cellular DNA. *Chem. Res. Toxicol.* **2006,** 19, 745-752

7 Culp, S. J., Poirier, M. C., and Beland, F. A. Biphasic removal of DNA adducts in a repetitive DNA sequence after dietary administration of 2-acetylaminofluorene. *En*V*iron. Health Perspect.* **1993**, 99, 273-275.

8 Cui, X. S., Eriksson, L. C., and Moller, L. Formation and persistence of DNA adducts during and after a long-term administration of 2-nitrofluorene. *Mutat. Res.* **1999**, 442, 9-18

9 Campbell, J., Crumplin, G., Garner, J.V., Garner, R.C., Martin, C.N. Rutter, A. Nitrated polycyclic aromatic hydrocarbons: potent bacterial mutagens and stimulators of DNA repair synthesis in cultured human cells. *Carcinogenesis*. **1981**, 2, 559-65

10 Moller, L., Lax, I., Eriksson, L.C. Nitrated Polycyclic Aromatic Hydrocarbons: A Risk Assessment for the Urban Citizen. *Environ Health Perspect*. **1993**, 101, 309 -315

11 Borlak, J., Hansen,T., Yuan,Z. Sikka, H.C., Kumar, S., Schmidbauer, S.Frank, H., Jacob, J., and Seidel, A. Metabolism and DNA-binding of 3-nitrobenzanthrone in primary rat alveolar type II cells, in human fetal bronchial, rat epithelial mesenchymal cell lines. *Polycyclic Aromat. Compds.* **2000**, 21, 73-86

12 Ostling, O., and Johanson, K.J., Microelectrophoretic study of radiation-induced DNA damages in individual mammalian cells. *Biochem. Biophys. Res. Commun.,* **1984,** 123, 291-8

13 Enya, T., Suzuki, H., Hisamatsu, Y. Reaction of benzanthrone (7H-benz[de,e]anthracen-7-one) with nitrogen dioxide alone or in admixture with ozone. Implications for the atmospheric formation of genotoxic 3-nitrobenzanthrone. *Bull. Chem. Soc. Jpn*. **1998**, 71, 2221-2228

14 Seidel, A., Dahmann, D., Krekeler, H., Jacob, J. Biomonitoring of polycyclic aromatic compounds in the urine of mining workers occupationally exposed to diesel exhaust. *Int. J. Hyg. Environ. Health.,* **2002**, 204, 333-338

15 Stiborova, M., Arlt, V.M., Henderson, C.J., Wolf, C.R., Frei, E., Schmeiser, H.H. and Phillips, D.H. Molecular Mechanism of Genotoxicity of the Environmental Pollutant 3-Nitrobenzanthrone. Biomed Pap Med Fac Univ Palacky Olomouc Czech Repub. **2005,** 149,191-7

16 Arlt, V.M., Stiborova, M., Henderson, C.J., Osborne, M.R., Bieler, C.A., Frei, E., Martinkek, V., Sopko, B., Wolf, C.R., Schmeiser, H.H., Phillips, D.H. Environmental pollutant and potent mutagen 3-nitrobenzanthrone forms DNA adducts after reduction by NAD(P)H:quinone oxidoreductase and conjugation by acetyltransferases and sulfotransferases in human hepatic cytosols. *Cancer Res*. **2005**, 65,2644-52

17 Arlt, V.M., Glatt, H., Muckel, E., Pabel, U., Sorg, B.L., Seidel, A., Frank, H., Schmeiser, H.H., Phillips, D.H. Activation of 3-Nitrobenzanthrone and its Metabolites by Human Acetyltransferases, Sulfotransferases and Cytochrome P450 Expressed in Chinese Hamster V79 Cells. *Int. J. Cancer*, **2003**, 105, 583-592

18 Arlt, V.M., Stiborova, M., Hewer, A., Schmeiser, H.H., Phillips, D. Human Enzymes Involved in the Metabolic Activation of the Environmental Contaminant 3-Nitrobenzanthrone: Evidence for Reductive Activation by Human NADPH:Cytochrome P450 Reductase. *Cancer Res*., **2003**, 63, 2752-2761

19 Arlt, V.M., Bieler, C.A., Mier, W., Wiessler, M., Schmeiser, H.H. DNA adduct formation by the ubiquitous environmental contaminant 3-nitrobenzanthrone in rats determined by ^{32}P-postlabeling. *Int. J. Cancer*, **2001**, 93, 450-454

20 Seidel, A., Dahmann, D., Krekeler, H., Jacob, J. Biomonitoring of polycyclic aromatic compounds in the urine of mining workers occupationally exposed to diesel exhaust. *Int. J. Hyg. Environ. Health.* **2002**, 204, 333-8.

21 Takamura-Enya, T., Kawanishi, M., Yagi, T., Hisamatsu, Y. Structural Identification of DNA Adducts Derived from 3-Nitrobenzanthrone, a Potent Carcinogen Present in the Atmosphere. *Chem. Asian J*. **2007**, 2, 1174-1185

22 De Los Santos, C. Probing DNA structure by NMR spectroscopy. *Comprehensive Natural Products Chemistry*. **1999**, 7, 55-80

23 Plum, G.E., Breslauer, K.J., Roberts R.W. Thermodynamics and Kinetics of Nucleic Acid Association/Dissociation and Folding Processes. *Comprehensive Natural Products Chemistry*. **1999**, 7, 15-53

24 Marky,L.A., Breslauer, K.J. Calculating thermodynamic data for transitions of any molecularity from equilibrium melting curves. *Biopolymers*. **1987**, 26, 1601-1620

25 Bohon, J., de los Santos CR. Effect of 6-thioguanine on the stability of duplex DNA. *Nucleic acids Res.* **2005**, 33, 2880-6